PERFORMANCE EVALUATION OF A GASIFIER COOLING JACKET BY MEANS OF A HOMOGENEOUS TWO-PHASE FLOW SIMULATION MODEL

G. Naudé

Dissertation in partial fulfilment of the requirements for the degree Magister Engineering at the Potchefstroom University for Christian Higher Education

Supervisor: **Prof. E.H Mathews**

2000

Potchefstroom

ABSTRACT

"PERFORMANCE EVALUATION OF A GASIFIER COOLING JACKET BY MEANS OF A HOMOGENEOUS TWO-PHASE FLOW SIMULATION MODEL."

SASOL II uses a number of coal-fired Gasifiers with water-cooled jackets to produce raw-gas for the purpose of manufacturing petroleum from coal. Excess heat generated by firing of the coal is removed with the aid of a water-cooled jacket. Cooling water circulates through the cooling system by means of natural convection only. During operation of this equipment, excessive deformation, or localised buckling of the Gasifier inner wall is experienced, due to localised overheating.

Three Gasifier water jacket concepts were devised to enhance the structural integrity of the Gasifier inner wall, and increase the cooling water mass flow rate. A one dimensional homogeneous steady state two-phase flow simulation model was developed to simulate the thermo-hydraulic performance of the Gasifier jacket concepts.

Boundary conditions including the heat flux profile, high-pressure boiler feed water inlet temperature and system pressure was specified to calculate (amongst other parameters) the rate of circulation, total pressure drop and heat transfer rate through the wall to the water. The Gasifier cooling system geometry was discretised and numerically solved by programming in a software package called Engineering Equation Solver.

Verification of calculated results proved that the model over estimates flow rates with a maximum error of 50 %, with the maximum error made when calculating temperature set at 8 %. The simulation results proved that the Box Belt concept combined with configuration 3a should be employed since it will provide the best performance, which is approximately 15 percent higher than the Base Case.

This study was industry driven, with production costs and equipment availability being the main research drivers. The usefulness of the homogeneous approach is also proven in this study with the estimation of complex system behaviour.

OPSOMMING

"WERKVERRIGTINGS EVALUASIE VAN 'N GASIFISEERDER VERKOELINGS ANNULUS DEUR MIDDEL VAN 'N HOMOGENE TWEE FASE FLOEI SIMULASIE MODEL."

SASOL II gebruik 'n aantal water verkoelde Gasifiseerders om afgas te produseer met die vervaardiging van petroleum uit steenkool. Verkoelings water sirkuleer deur die Gasifiseerder sisteem deur middel van natuurlike konveksie. Lokale oorverhitting van die binne wand van die Gasifiseerder veroorsaak plastiese deformasie, met resulterende produksie verlies en hoë herstel koste.

Drie water mantel konsepte is ontwikkel om eerstens die strukturele integriteit van die binne wand van die Gasifiseerder te verhoog, en tweedens die verkoelwater vloeitempo te verhoog. 'n Een dimensionele gestadigde twee fase floei simulasie model is ontwikkel om die termo-hidrouliese werksverrigting vand die Gasifiseerder verkoel water mantels konsept te evalueer.

Randwaardes wat die hitte vloed profiel, hoogdruk stoomketel voer water inlaat temperatuur en stelsel druk is gespesifiseer om onder andere verkoel water vloeitempo, totale druk verlies en hitte oordrags tempo van die wand na die water te bereken. Die Gasifiseerder verkoelings stelsel is gediskretiseer en numeries opgelos deur gebruik te maak van 'n sagteware pakket bekend as Engineering Equation Solver.

Die verifikasie van die simulasie model het aangedui dat die model vloei tempo's met 'n maksimum fout van 50 % oorskat, terwyl die foutgrens met temperatuur berekenings op 8 % te staan gekom het. Die simulasie resultate het bewys dat die Boks belt konsep in kombinasie met konfigurasie 3a die beste Gasifiseerder werkverrigting lewer, wat ongeveer 15 % beter as die huidige Gasifisserder verkoel water konfigurasie is.

Hierdie studie was industrie gedrewe met produksie koste en toerusting beskikbaarheid die hoofredes waarom die studie voltooi is. Die nuttigheid van die homogene simulasie benadering met die modelering van 'n komplekse sisteem word deur die verhandeling bewys.

TABLE OF CONTENTS

LIST OF FIGURES

LIST OF TABLES

CHAPTER 1: INTRODUCTION

1. Introduction

Although two-phase flows are commonly encountered in many industrial applications, it is still one of the most intricate phenomena to describe analytically during the design process. The simultaneous flow of a gas and a liquid occurs in a multitude of industrial applications, and is commonly accompanied by heat and mass transfer. Detailed analysis and research of two-phase flow phenomena originally seeded from the nuclear industry, as safety demands are high due to the inherent negative effects of nuclear power on both nature and the human being.

The nuclear power industry falls beyond the scope of this dissertation however, research from the latter field will be implemented to aid with analysis of Gasifying equipment used by SASOL II. A brief background on the particular application and problems that seeded this particular dissertation will be outlined first. A broad overview of two-phase flow phenomena and the characteristics, advantages and limitations of the basic types of model assumptions will be discussed thereafter in an effort to identify the most suitable modelling approach to be followed.

Most of the information contained in this chapter was taken from the text book by Levy *(1999)* who is a world renowned specialist on the field of two-phase flow phenomena, and one of the leading consultants in the investigation of the Three Mile Island Accident.

1.1 PHYSICAL PROBLEM BACKGROUND

SASOL II uses a number of coal-fired Gasifiers with water-cooled jackets to produce raw-gas for the purpose of manufacturing petroleum from coal. Figure 1.1 shows a cross sectional view of the Gasifier and terminology that will subsequently be used in the remainder of this document. The working principal of the Gasifier will be explained for the sake of understanding difficulties experienced during the operation of this equipment, and to define the need for research.

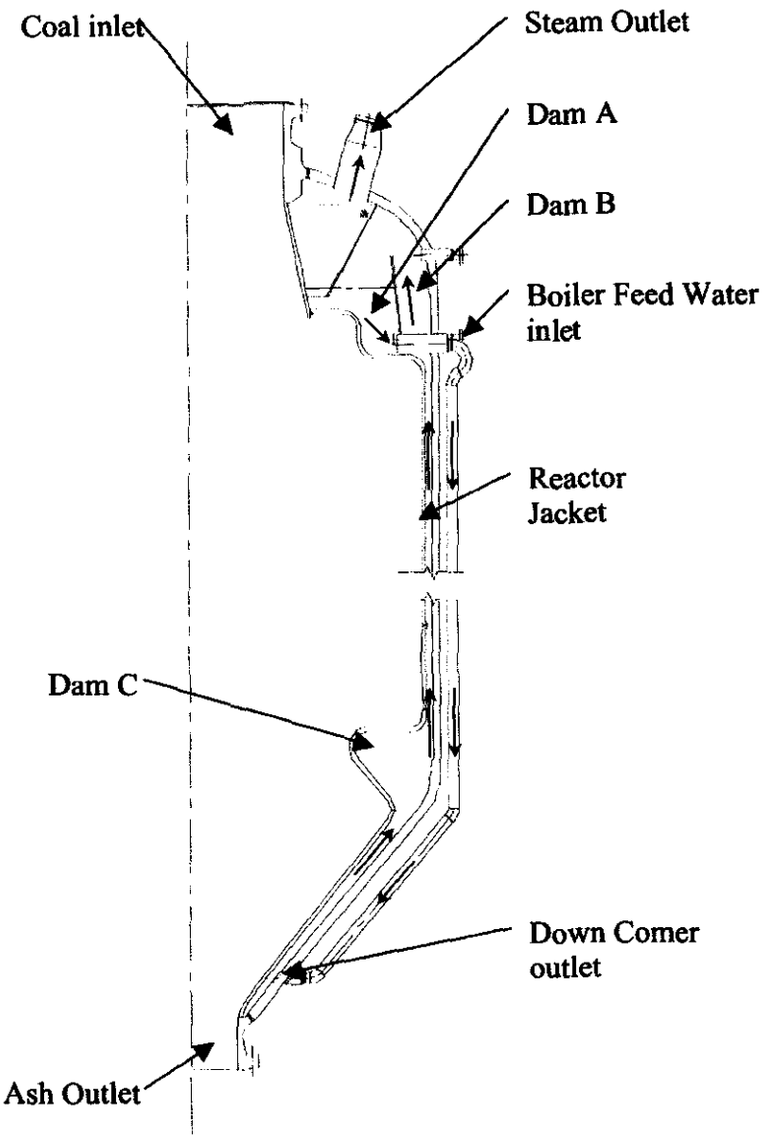

Figure 1.1: General arrangement of the Gasifier.

Coal is fed through the coal inlet at the top as shown in Figure 1.1, and burnt within the gasifier. Excess heat is removed from the gasifier system by means of a water-cooled annulus formed between the gasifier inner- and outer walls, for the purpose of preservation of the inner and outer wall integrity of the system. Boiler feed water is fed through the boiler feed water inlet pipe at a mass flow rate of 12 tons per hour, at an inlet temperature of 105 °C into dam A, as shown in Figure 1.1.

The system is operated at a pressure of 3040 kPa. Three 'down comer' pipes feed water from dam A at the top through natural convection only, to the bottom of the Gasifier. Heat transfer through the Gasifier wall causes a change in density of the cooling water, consequently causing water to be forced upwards along the cooling water annulus as the inner Gasifier wall temperature increases. A mixture of steam and water enters dam B, with dry steam escaping through the Steam outlet of the Gasifier. A perforated cone guides water condensate back to dam A, and the cycle repeats itself.

During operation of this equipment, excessive deformation, or localised buckling of the Gasifier inner wall is experienced. Sections of approximately 1.5 meters wide and 4.5 meters tall bulge inwards due to the pressure differential between the cooling water annulus and Gasifier inner wall, and is considered as a system failure. Such a Gasifier has to be taken off-line to enable the repair of the Gasifier inner wall, and subsequently has a negative impact on plant production due to down time on the Gasifier section. Furthermore, excessive repair costs are experienced during the repair of the latter failure, having a detrimental impact on production costs and company revenue. This however, falls beyond the scope of this dissertation.

1.1.1 Gasifier Cooling Water Jacket Designs

The original Gasifier design as proposed by LURGI, utilises a 25 mm thick inner wall with an annulus depth of 46 mm, as shown in Figure 1.2. This will be referred to as the 'Base Case' during the remainder of this dissertation, and evaluation of the Gasifier performance will be done against the latter.

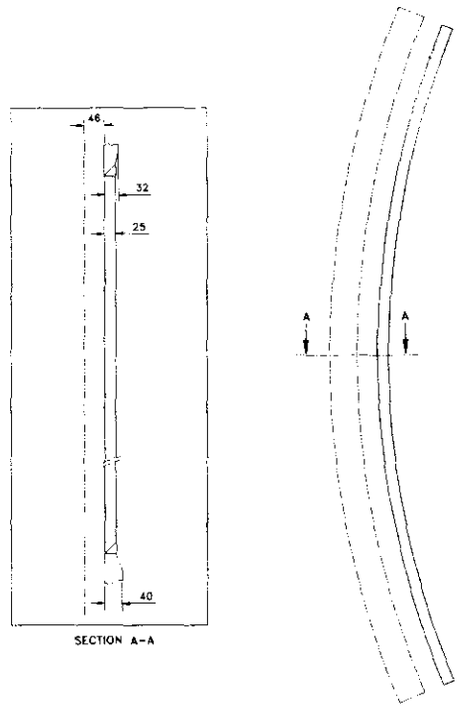

Figure 1.2: Cross sectional view of the Base Case Gasifier jacket.

Localised overheating of the jacket inner wall causes the mentioned sectional failures of the Gasifier Cooling water jacket. Two means of solving the problem could be devised.

- The first would be to reconsider system-operating parameters, like changing the system operating pressure in the water cooling annulus geometry for an instance, with subsequent investigation of localised boiling regimes that exists within the water annulus. However, this is a function of down stream steam and raw gas process requirements and could not readily be changed.
- Secondly, the inner Gasifier wall structural integrity could be enhanced with the addition of 'stiffening rings' along the periphery of the Gasifier inner wall in the cooling water annulus. This would also entail detailed analysis of Gasifier inner wall temperatures, investigation of the predominant boiling regimes at the surface of the Gasifier inner wall, and the influence of the stiffening rings on the steam production of the Gasifier system.

SASTECH, the technology division of SASOL, proposed a detail investigation of the effect of the concept stiffening rings on the thermal hydraulic properties of the Gasifier. Three Gasifier jacket concepts were proposed by SASTECH:

- *Box Belt Gasifier Jacket:* The Box Belt Gasifier jacket consists of a thinner 12 mm thick inner wall, as shown in Figure 1.3.Twenty four vertical channels are welded along the periphery of the Gasifier inner wall, and are interconnected by means of 5 horizontal belts within the cooling water annulus.
- *Belt jacket A:* The wall thickness with this concept remains 12 mm as with the Box Belt Gasifier Jacket Concept. Five T-shaped stiffener rings are welded horizontally along the periphery of the Gasifier inner wall and the web of the T-sectioned stiffening rings in the cooling water annulus. A number of holes are drilled through the web of the T-section in an effort to minimise pressure drop across the stiffening rings.
- *Belt Jacket B:* As with the previous concepts, the inner wall thickness of the Gasifier jacket remains 12 mm thick. Five Channel shaped stiffener rings are welded horizontally along the Gasifier inner wall periphery and channel flanges in the cooling water jacket annulus. A number of holes are drilled through both flanges of the stiffening rings to minimise the induced pressure loss by the additional stiffening rings.

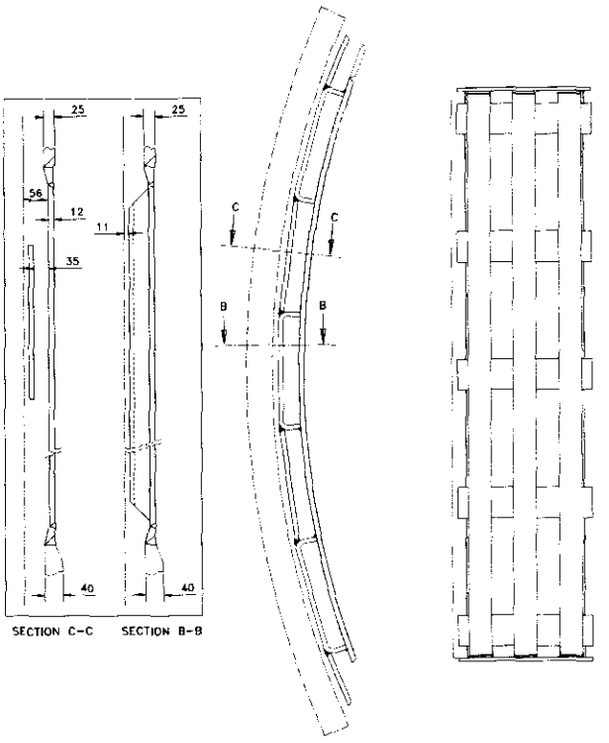

Figure 1.3: Cross sectional view of the Box Belt Gasifier jacket with reduced wall thickness.

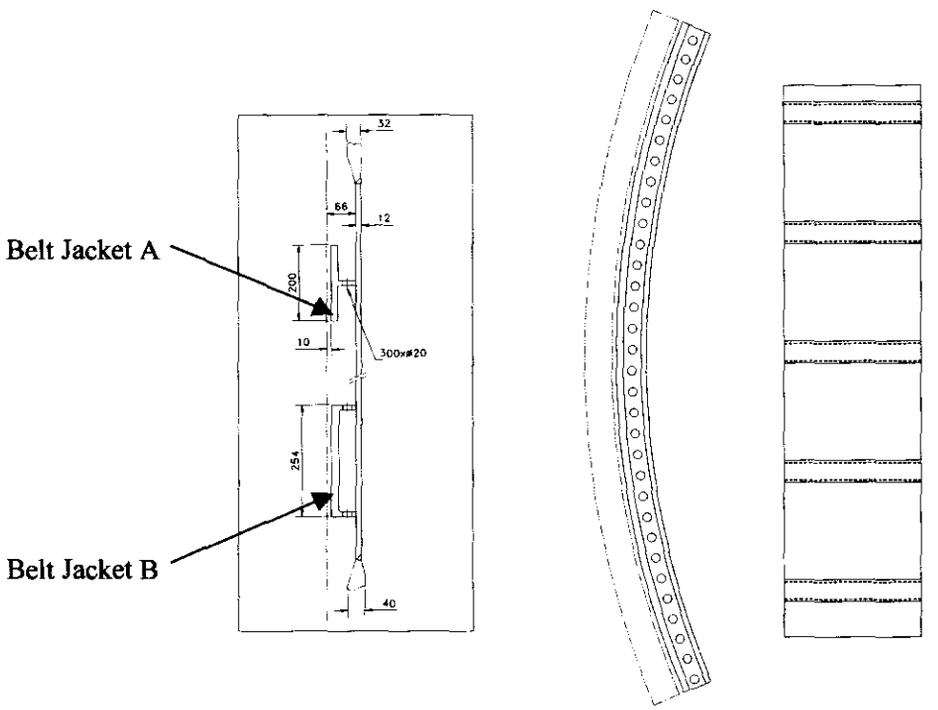

Figure 1.4: Cross Sectional view of the Belt Jacket A and Belt Jacket B Gasifier jacket concepts.

Furthermore, four different boiler feed water inlet configurations will be considered, for each of the above mentioned Gasifier Cooling water jacket concepts, in an effort to identify a configuration that ensures maximum heat transfer. Four different boiler feed water inlet configurations are distinguished, and are depicted in Figure 1.5.

- *Configuration 1:* Boiler feed water is injected directly into dam A, which is currently the most prevalent configuration used on the majority of the Gasifiers on SASOL II.
- *Configuration 2:* A common ring type header connects the top of the three equally spaced down comers, with the boiler feed water injected into the mentioned common ring. Therefore, supply water will consist of excess water that did not evaporate in the cooling water jacket; steam condensate and high-pressure boiler feed water.
- *Configuration 3a:* In this configuration, boiler feed water is injected into the bottom of the down comer, with the supply water consisting of water from dam A, and boiler feed water.
- *Configuration 3b:* The down comers are removed from the Gasifier, and boiler feed water is injected directly into the bottom of the Gasifier annulus.

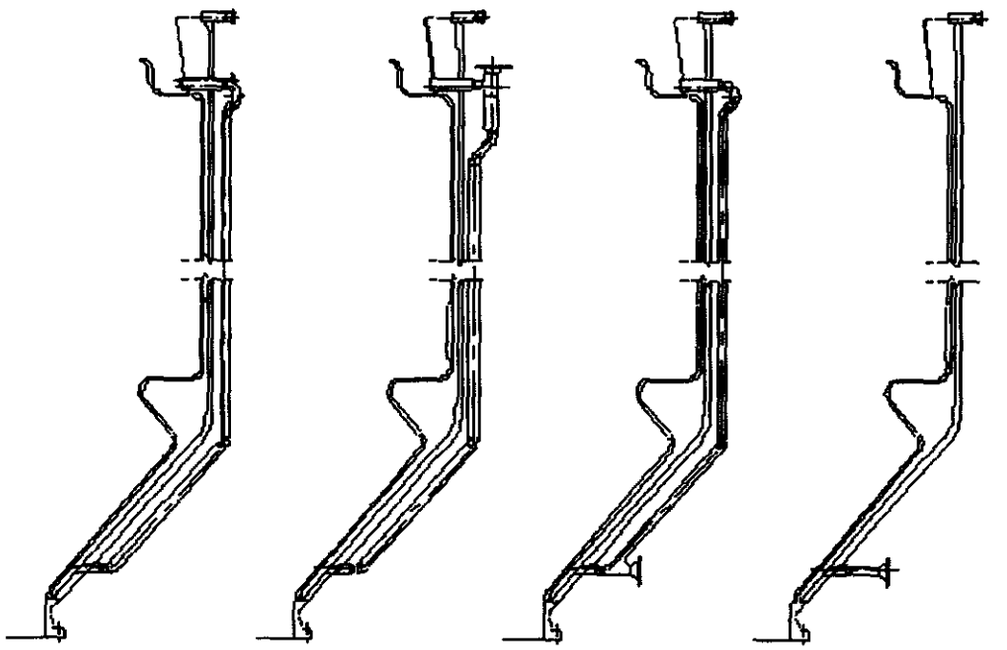

Figure 1.5: Boiler Feed water inlet configurations.

Sixteen different configurations will be analysed based on results obtained from a thermal hydraulic simulation model. Temperatures in the Gasifier inner wall will result in a phase change in the cooling water from the liquid- to a mixture of the liquid- and gas- states, or to a pure gas-state. Thus, two-phase flow theory and models will be considered in the ensuing paragraphs.

1.2 BACKGROUND ON TWO-PHASE FLOW

A variety of computer codes have been developed to analyse, design and operate complex two-phase flow systems. Two-phase flow computer codes must not only be able to simulate several sub-systems, components and their couplings, but also has to deal with the simultaneous occurrence of various two-phase phenomena and processes. Associated two-phase flow phenomena are to a great extent more complicated than single-phase flow phenomena. To gain a better understanding of the underlying complexity of two-phase flow systems, a few fundamental problems will be discussed below.

Three properties that are essential to the solution of thermo-hydraulic systems are density, thermal conductivity and viscosity. In single phase-flow these properties are usually known or can be calculated at any point along the flow in a channel. In two-phase flow however, the liquid and gas phases usually do not have the same local velocity. Consequently, fluid density cannot be calculated directly from the total liquid and gas flow rates specified. Furthermore, no generally accepted expression exists for the viscosity or thermal conductivity of a gas-liquid mixture. This adds to the complexity of two-phase flow solutions.

A very large number of gas-liquid interfaces are present in two-phase flow systems. At each of these gas-liquid interfaces, momentum, mass and energy are transferred from one phase to another. This has a profound effect on two-phase flow predictions. The transfer mechanisms and areas over which they occur are very difficult to specify or measure. The presence of gas-liquid interfaces and the difficult task of describing it, was and will probably continue to be the weakest element in developing reliable generic two-phase flow system computer codes.

Two-phase flow usually contains a large variety of flow patterns that are dependant on pipe geometry and flow properties like gas- and liquid- velocities. These flow patterns are divided into five major groups, which include:

- *Bubble flow* - Gas bubbles of variable shape and size contained in a non-homogenous liquid phase.
- *Stratified flow* - Liquid droplets dispersed in a non-homogenous gas phase
- *Slug flow* - Large gas bubbles almost filling the channel, separated by slugs of liquid.
- *Annular flow* - A liquid film surrounding a homogenous or non-homogenous gas phase.
- *Stratified flow* - A Homogenous liquid- and gas-phase, geometrically separated by a phase interface with or without waves at the interface.

These two-phase flows can furthermore be in transition from one pattern to another, which are known as *slug* and *churn* flow patterns.

All two-phase flow patterns are discontinuous in their overall and local time behaviour. In comparison with single-phase flow, two-phase flow exhibits significantly larger variations with time. In bubble flow the local gas- or void fraction fluctuates between zero and unity in a sporadic manner, whereas annular and stratified flow experience waves of different amplitude and shape at the interface. The periodic changes in phase content experienced when encountering slug flow can be large, while the flow direction in churn flow can even alternate. Values of fluid density, pressure drop and heat transfer can also be expected to vary with the flow pattern encountered. This necessitates a family of approximate solutions to match all possible types of flow patterns and the transition from one pattern to another.

Two-phase flow has numerous other degrees of freedom that do not occur in single-phase flow. According to Levy *(1996)*, they include:

- *Co-current and counter-current flow can occur.* In co-current flow the liquid and gas are flowing in the same direction while in *counter-current* flow the liquid and gas are flowing in opposite directions. Both the behaviour and transfer mechanisms at the interfaces differ for *co-current* and *counter-current* flow.
- *Thermal non-equilibrium* can exist between the two phases. When heat is added or removed at a boundary surface with a temperature above the fluid saturation temperature, vapour bubbles may exist at the boundary surface even though the main stream is sub-cooled. An inverted annular flow pattern could result if the surface temperature is high enough, and the resulting vapour does not condensate. Superheated vapour will be found next to the heated surface, with a saturated or sub-cooled liquid core inside the superheated vapour annulus. Other thermal non-equilibrium phenomena, like superheated dispersed vapour containing saturated liquid drops (inverted dispersed flow), or a saturated condensing liquid film in contact with superheated steam can occur in two-phase flows.

Clearly the transfer mechanisms, flow patterns and interface behaviour can be expected to require special treatment for these thermal non-equilibrium conditions.

The issues addressed above should make it clear that generic computer codes cannot be expected to deal with detailed fully transient flow patterns on an in-time basis but rather the time-averaged characteristics. It is also important to note that due to the complexity of two-phase flow models, most of the existing computer codes only allow for the simulation of very specific flow patterns and/or fluid combinations.

Three distinctive approaches to model two-phase flow has been identified from the literature survey. They are:

- Homogenous two-phase flow models.
- Separated or mixture two-phase flow models with no interface exchange.
- Two-fluid models including interface exchange.

1.3 OVERVIEW OF TWO-PHASE FLOW MODELS

1.3.1 Homogenous Two-Phase flow models

1.3.1.1 BASIC MODEL CHARACTERISTICS

Levy *(1996)* defines homogenous flow as one where the two-phase fluid properties are taken to be constant over the cross sectional area and the liquid and gas velocities as well as temperatures are equal. This implies that all the fluid properties, for example the specific volume, weight rate fraction, thermal conductivity and viscosity, are assumed to be constant over the cross section. Effective fluid properties are defined in terms of the weighted average fluid properties.

It is also assumed that both phases are subjected to the same local pressure. The three independent variables namely specific enthalpy, average gas velocity and local pressure, are taken to be functions of position along the length of the duct or pipe.

Boundary conditions used in homogenous two-phase flow models are based on a methodology similar to that used for single-phase flow. The pressure drop along an element is derived from the steady-state homogenous equations. The laminar homogenous friction factor and homogenous turbulent shear stress has the same form as for single-phase flow. Prandtl's mixing length theory is implemented to obtain the mean fluid velocity, in conjunction with an empirically derived equation to calculate an approximate value for the mixing length and the mean homogenous velocity. A correlation based on the well-known chart presented by Moody *(1944)*, is used to obtain the friction factor. This is applicable to both circular and non-circular geometries by employing the concept of hydraulic diameter.

The homogenous model conservation equations are identical to the conservation equations applicable to single-phase flow. This is not surprising since a truly homogenous two-phase system with constant fluid properties can intuitively be expected to behave like single-phase fluid flow. It has to be noted that single-phase closure equations are derived for steady state, fully developed flow conditions. However, these equations are also generally used in all complex two-phase flow system computer codes, even where transient conditions prevail.

The average homogenous two-phase fluid viscosity is a function of the average gas weight flow fraction. Consequently, the homogenous Reynolds number is equal to the sum of the liquid and gas Reynolds numbers. The average homogenous viscosity can also be calculated using the average gas volume fraction as implemented by Bankoff *(1960)*. Four other equations have been identified that describe the latter property, each with it own limitations. Merilo et al. *(1977)* proposed a correlation for the thermal conductivity of a liquid gas pool. These correlations are usually combined with the assumption that the conductivity of the gas is small compared to that of the liquid.

1.3.1.2 ADVANTAGES AND LIMITATIONS

Based on the discussion above, the following advantages and limitations can be identified:

- Homogenous two-phase flow does not have to deal with gas-liquid interfacial interactions. The fact that homogenous conservation equations are derived from equations similar to single-phase flow implies that empirical correlations for single-phase flow can be employed. Therefore, no new boundary conditions have to be defined for a homogenous/uniform property computer code.
- The homogenous flow assumptions become more accurate when the liquid and gas properties approach each other. This happens near to the critical pressure for a single component fluid. These models can also be more readily used to describe two-phase flow at very high velocities and pressure drops. The homogenous two-phase flow model has also been used effectively to predict dispersed flow of liquid drops in a gas stream.
- Homogenous two-phase flow models require expressions to calculate viscosity and thermal conductivity. Preference should be given to those equations that satisfy the property values at 100 % gas or liquid flow.
- Consistency is of great importance in implementing homogenous two-phase flow models. The model would be inaccurate if a single-phase closure law based on uniform property conditions is combined with liquid properties on the bounded surface. Inconsistency will also be observed if the average gas volume fraction is obtained from an equation that assumes different gas and liquid velocities but implemented along with homogenous flow equations for pressure drop and heat transfer.

- Homogenous computer codes are easier to implement and take less time to run.
- The principal shortcoming is presuming equal gas- and liquid- velocities as well as equal gas- and liquid-temperatures. However, if implemented correctly, this model can be valuable in estimation/scaling of complex system behaviour.

1.3.2 *Separated two-phase flow models with no interface exchange*

Separated two-phase flow models without interface exchange may be used as a valuable substitute for the homogenous model. The main improvement is that it can be extended to include heat transfer when unequal gas- and liquid- velocities prevail. Separated two-phase flow models without interface exchange are formulated in terms of area-averaged and time-averaged flow parameters. Equal gas- and liquid- temperatures are assumed.

Omitting interface exchange effects cause the models to rely on semi-empiric or empiric equations to calculate the gas volume fraction, friction pressure drop, and heat flux at the boundary surfaces. Furthermore, the model is derived analogous to single-phase models, assuming uniform fluid property values across the flow area. This includes the gas volume fraction.

An approximate two-phase frictional pressure drop is defined in terms of the homogenous density and momentum density, discarding the effect of fluid viscosity. This parameter is used to permit the model to incorporate unequal fluid- and gas- velocity. However, these models are still inherently simple when coupled to an uncomplicated gas volume fraction relation.

The main limitations of separated two-phase flow models without interface exchange can be blamed on discarding the two-phase microstructure at the interface.

1.3.2.1 MARTENELLI SEPARATED MODEL

1.3.2.1.1 LOCKHEART-MARTENELLI MODEL

The Lockheart-Martenelli model *(1949)* describes liquid- and gas-velocities separately with the presumption that losses in the liquid and gas phases can be calculated from single-phase relations. Hydrostatic losses were also neglected because of the dominance of friction or other pressure drops that occurs for example in flow through a valve. It is also assumed that the static pressure-drop in the fluid and gas phases is equal.

This assumption is made to define a dimensionless frictional parameter in terms of the gas average volume fraction, stagnation pressure, liquid phase pressure and gas phase pressure. A single curve for the gas- and liquid average volume fraction can therefore be calculated. Four equations were derived for different combinations of the frictional parameter based on different combinations of laminar and turbulent gas- and liquid- flow.

The Lockheart-Martenelli model involves many assumptions, but gives good results for two-phase pressure drop and gas volumetric fraction. This is however only true for conditions which coincide with test conditions. The main advantage is the use of its liquid- and gas-fluid properties that leads to avoidance of invalidated expressions for two-phase fluid properties.

1.3.2.1.2 MARTENELLI-NELSON MODEL

Martenelli and Nelson *(1948)* extended the Lockheart-Martenelli friction parameter correlation to the turbulent flow of steam-water mixtures. At pressures near atmospheric conditions the correlation data compares well with empirical data, but overestimates empirical results at high pressures.

1.3.2.2 OTHER TWO-PHASE SEPERATED FLOW MODELS WITHOUT INTERFACE EXCHANGE

A number of analytical and empirical correlations have been researched and extended to make the Lockhart-Martenelli model applicable to a broader range of two-phase flow patterns. These include:

- The analytical exchange model by Levy *(1996)*, and the energy model proposed by Gopalikrisham and Shrock *(1964)* express the gas volume fraction in terms of the weight rate fraction. These correlations are simple, but not accurate.
- Friedel *(1987)* has developed an empirical correlation for the frictional pressure drop parameter that is only applicable to two-phase flow, for any fluid where the gas phase viscosity is one thousand times smaller than the liquid phase viscosity. The CISE correlation was the most accurate correlation for the gas volume fraction, but the ERPI correlation proposed by Lellouche et al. *(1986)* is currently considered the most accurate. The Friedel, CISE and EPRI expressions can be implemented when data lacks in a complex system.
- In general, customized empirical correlations developed for specific conditions are preferred over analytical counterparts, and are considered to be the most accurate.

1.3.2.3 DRIFT FLUX MODEL

The drift flux model is another type of separated flow model. It considers the volumetric flux of each phase and not the gas- and liquid- velocities. The drift flux model takes non-uniform distribution of the phases and two-phase phase velocity (sum of the liquid and gas velocities) into account. It also considers the difference between the velocities of the gaseous phase with respect to the two-phase velocity (referred to as the drift velocity).

The drift flux model also incorporates the effects of flow pattern with correlations for slug flow, bubble flow and annular flow. These correlations make it possible to calculate the average volume fraction from two-phase stream properties. This enhances the usefulness of the drift flux model. The drift flux model incorporates the degree of thermal equilibrium, channel characteristics, flow direction, as well as total mass flow.

Many attempts have been made to predict the drift flux gas volume fraction, and the most extensive is the EPRI correlation. This correlation is applicable to all flow patterns and flow directions, but varies in form for different fluids considered. RELAP5/MOD3 uses this correlation to predict the behaviour of systems subjected to two-phase flow.
The EPRI correlation is the result of an intensive effort to fit available data over a number of gas-liquid flow conditions.

1.3.2.4 ADVANTAGES AND LIMITATIONS

- The Martenelli models proved to be useful in predicting transient behaviour of complex systems. Inherent model simplicity contributes to ease of implementation, and proves to be reasonably accurate as long as it is used under conditions for which the models apply.
- Models that do not include special two-phase fluid property relations are preferable, and contribute to the simplicity of these models. However, these models are not accurate and should not be applied in conditions outside its range of applicability. The empirical nature and incompetence to deal with two-phase structure are reasons for inaccuracy encountered with these models.
- The drift flux model has numerous advantages over other separated flow models which include:
    - The drift flux model incorporates the local phase velocity difference. This means that it does not include the difference of average gas and liquid velocities, which contribute to an improved accuracy of the model. The drift flux model describes physical two-phase flow realistically.
    - The drift flux model takes the flow distribution in the channel into account, by incorporating the EPRI correlation. It also incorporates the effects of flow pattern in the model. However, simplicity is forfeited with the addition of more flow pattern correlations. Decreasing simplicity implies increasing accuracy.
    - Drift flux models are inherently capable of handling co-current or counter-current flow, and counter-current flow limitations.

1.3.3 Two- fluid models including interface exchange

Two-fluid models include interface interaction. This implies that these models incorporate different gas- and liquid-velocities, dissimilar gas- and liquid-temperatures and consider the effects of co-current and counter-current flow. These models still rely on one-dimensional formulations and time- and spatial-averaging. Therefore, they do not consider variations in fluid properties like velocity- and temperature gradients at the wall and interface boundaries.
These models use property correlations to include the above-mentioned effects at the interface and wall boundaries.

It is well known that property correlations are dependant on flow patterns, which necessitates the inclusion of flow regime maps. The conservation laws, based on the set proposed by Yadigroglu and Lahey *(1987)* allow liquid to be transferred into the gas, or visa versa. These equations permit the inclusion of property transfer at the wall boundary and interface. These models furthermore include phase specific net pressure forces, as well the effects of gravitational force in a complex system.

It also integrates the interface- and wall shear stresses and momentum addition caused by mass transfer from one phase to another. A virtual mass term is introduced to include the effects of the force required to accelerate the apparent mass of the surrounding phase, when a difference in phase velocities occur. The virtual mass term is only significant for quick flow changes, and its primary function (for non-critical flow) is to stabilize the numeric solution.

The phases are presumed to be at the same pressure, but this assumption is invalid for stratified flow. In the case of stratified flow, a pressure difference does exist and must be taken into account to determine interfacial instability and the transition from stratified- to slug flow. The conservation laws may thus be inadequate to include the effects of intermittent flow in a complex system.

Furthermore, a total of thirteen expressions must be provided to calculate the volumetric mass exchange, wall shear force applied to each phase, interfacial shear force, the heat supplied from the wall to each phase, and interfacial energy transfer rates. When considering a heat balance at the interface it becomes apparent that an additional ten equations must be supplied to describe fluid properties like heat flux and enthalpy difference.

1.3.3.1 INTERFACE AND WALL SHEAR

1.3.3.1.1 INTERFACIAL SHEAR AREA AND SHEAR STRESS

To compute interfacial shear forces and stresses at wall boundaries and interfaces, interfacial shear area has to be computed. It was found that many geometric and other assumptions have been made to enable the computation of the interfacial shear area. For example, in computing the interfacial shear area for bubble- and stratified flow, the assumption has been made that spherical bubbles and droplets with specified size exist in the flow.

When one of the phases for example assumes two forms, the interfacial area is computed by adding the interfaces. This implies that the two forms behave the same at the interfaces. A detailed set of models to compute interfacial areas and shear forces does not exist for all flow regimes.

Interfacial area and shear stress equations were derived from adiabatic steady-state test conditions. These are applied with the assumption that they are applicable to transient and heated conditions.

1.3.3.1.2 WALL SHEAR

The wall shear prediction in system codes with interfacial exchanges relies on empirical correlations. These are not always consistent with the interfacial perimeter and gas volume fraction values. These empirical correlations furthermore vary from one computer code to another.

1.3.3.2 INTERFACIAL AND WALL HEAT TRANSFER

Several heat transfer regimes have to be considered on boundary walls and interfaces namely:

- Single-phase liquid or single-phase gas forced convection and single-phase liquid or single-phase gas natural convection.
- Gas-liquid mixture forced or gas-liquid mixture natural convection.
- Nucleate boiling up to the point of critical heat flux where the heated surface are no longer fully wetted.
- Transition boiling where the heated surface is alternately covered by liquid and vapour.
- Film boiling where the heated surface is alternately covered by liquid and vapour.
- Condensation where vapour is converted back to liquid.

Idealized geometries, empirical correlations and interactions between phases are presumed to exist. Furthermore, it is assumed that the liquid and gas-phases are well mixed and at the same temperature.

From the preceding discussion it is apparent that two-fluid models including interface exchange are more complex and therefore generally more difficult to implement than the other two types discussed earlier.

1.4 SUMMARY

The following main issues have been identified:

- Progress has been made in the development of computer codes with models predicting two-phase flow on a physical basis. These codes still rely on a wide range of empirical relations obtained under steady-state conditions, which are not accurate under all conditions. This can be blamed on insufficient description of gas-liquid interfacial geometries and motion and deformation with time. The limitations imposed by these assumptions have been partially overcome by utilizing:
    - time- and cross sectional fluid property averaging,
    - property relations for mass, momentum and heat transfer to calculate missing information at the interface,
    - empirically based wall process models, and
    - flow regime maps.

  The weakest link in two-phase flow models is the lack of methods to correctly describe interface topology.
- Two-phase flow models can be divided into the following main groups:
    - Uniform homogenous two-phase flow models that presume equal gas and liquid velocity. These models require expressions for the homogenous viscosity and thermal conductivity. Uniform homogenous models use single-phase boundary property relations. These models offer a simple but important tool for estimation and scaling two-phase flow effects in complex two-phase flow systems.
    - Separated two-phase flow models with no interface exchanges also account for unequal gas- and liquid-velocities. These models are sufficient to predict two-phase flow in complex systems under normal and less severe transient conditions.
    - Drift flux and separated two-fluid flow models, which incorporates interface exchange require flow regime maps and boundary equations to define interfacial areas and mass-, momentum- and energy transfer. These models provide the most accurate prediction of two-phase flow because they describe the prevailing physics.
- The number of boundary equations and required empirical correlations grow in a near exponential fashion when proceeding from homogenous models towards the more complex two-fluid models with interfacial exchange.

1.5 DISCUSSION

As mentioned in the introduction of this chapter, research on two-phase flow was spawned by the discovery of nuclear power and the accompanying safety standards set by authorities. The degree of testing and analysis are extensive and challenging due to the critical consequences suffered during nuclear power plant failures.

Gasification by means of the installed Gasifier section at the SASOL II plant, in Secunda is of less critical extent with business considerations being the main driver for further research on this particular equipment, without compromising safety. As illustrated in the literature survey, the prevailing physics of two-phase flow systems are intricate and complex. Researchers still rely heavily on empirical relations, making the simulation of a two-phase flow system application specific. These empirical relations are furthermore obtained under steady state conditions, which further contribute to inaccuracy.

As already mentioned, three main simulation approaches can be identified with increasing complexity namely Uniform homogenous two-phase flow models, Separated two-phase flow models with no interface exchange, Drift flux and Separated two-phase flow models with interface exchange. The uniform homogenous two-phase flow approach is in the opinion of the author sufficient for the performance evaluation of the Gasifier. A system performance approach rather than a two-phase flow phenomena study are demanded by this particular problem, thus permitting the latter opinion. The objective of this study will be defined next.

1.6 OBJECTIVE

This particular study is devoted to the numerical simulation of the Gasifier as a system by means of a steady-state uniform homogenous two-phase flow model. Key Performance Indicators or KPI's are identified that is relevant to the SASOL process that includes the following:

- System total pressure,
- Volume flow rate in the three down-comers,
- Temperature in dam A,
- Water temperature at six different locations in the Gasifier jacket annulus at 0.5-meter intervals,
- Temperature on the down comer skins at the dam outlet, mixed stream and bottom re-entry inlet temperatures,
- Boiler feed water mass flow rate, and
- Total steam production.

These KPI's are physically measured and compared to serve as a validation of the simulation model and error margins will be quantified. Discretisation of the Gasifier geometry are discussed as well as boundary conditions that are specified as inputs to the numerical model. The different Gasifier cooling water jacket concepts are analysed along with the mentioned down comer configurations and traded off against each other.

An optimum solution are proposed, i.e. the Gasifier cooling water jacket that has the least profound influence on system performance in terms of the identified KPI's. Recommendations are made pertaining further identified work that might flow from this particular study.

1.7 REFERENCES

BANKOFF, S. G. 1960. A variable density single fluid model for two-phase flow with a particular reference to steam-water flows, Trans. ASME, Ser. C, vol. 82, p.265

CHEXAL, B., and LELLOUCHE, G., 1986. A full range drift flux correlation for vertical flows, EPRI Report NP-3989-SR, Rev. 1

FRIEDEL, L. 1987. Improved friction pressure drop correlations for horizontal and vertical two-phase flow, paper presented at the European two-phase flow group meeting, Ispra, Italy, 1979. Also, P.B. Whalley, Boiling, condensation and gas- liquid-flow, Oxford Science Publications, Oxford, Appendix B

GOPALAKRISHAM, A. and SCHROCK, V.E., 1964. Void fraction from the energy equation, Heat Transfer and Fluid Mechanics Institute, Stanford University Press, Palo Alto

LEVY, S. 1999. Two-phase flow in complex systems, USA: John Wiley & Sons. p. 86-155.

LOCKHART, R. W., and MARTENELLI, R.C., 1949. Proposed correlation of data for isothermal two-phase two-component flow in pipes, Chem. Eng. Prog., vol. 45, pp.34-48.

MARTENELLI, R. C. and NELSON, D. B., 1948. Prediction of pressure drop during forced circulation boiling of water, Trans. ASME, vol. 70, pp. 695-702

MERILO, M., DECHENE, R. L., and CHICOWLAS, W. M., 1977. Void fraction measurement with a rotating electric field conductance gauge, Trans. ASME, vol. 99, p.330

MOODY, L.F. 1944. Friction factors for pipe flow, Trans. ASME, vol. 69, pp. 947-959

YADIGAROGLU, G. and LAHEY, R. T., Jr. 1987. On the various Forms of the conservation equations in two-phase flow, Int. J. Multiphase Flow, vol. 2, pp.477-494

CHAPTER 2: IMPLEMENTATION OF A HOMOGENOUS TWO-PHASE FLOW MODEL

2. Introduction

This chapter will disclose the detailed equations implemented in the Homogenous steady state two-phase flow model used to simulate the flow by natural convection in the Gasifier as discussed in the previous chapter. As already mentioned, the following equations have been programmed using Engineering Equation Solver or EES where after the discretised geometry have been contained in Lookup tables. Particular detail surrounding the discretisation of the Gasifier geometry will follow in the next chapter.

2.1 SIMULATION APPROACH

One-dimensional flow models only take variations in the direction of flow into account, and ignore fluctuations in the other two spatial dimensions and also disregard any changes that might occur with time. This implies that the one-dimensional approach disregards changes in fluid properties around the perimeter of the Gasifier when viewed from the top.

Therefore, the flow path is discretised in the axial flow direction; with the independent variables namely mass flow rate, specific enthalpy and static pressure assumed to be functions of position only. Thus, the total flow area of the jacket when viewed from the top is assumed to be one single flow area combined into one single flow element. Furthermore, the three down comers situated along the outer perimeter of the Gasifier are also combined into a pseudo element with an equivalent diameter of three down comers in parallel.

This approach accounts for actual flow velocities, pressure drops and hydraulic diameters per discretised element. As will be indicated further in more detail in this chapter, pressure drop are calculated as a function of the Reynolds number applicable to that particular discretised element as well as secondary pressure loss coefficients describing the geometry for that particular element, similar to single phase flows.

Homogenous two-phase flow implies that fluid properties are assumed to be constant over any cross sectional area of the one-dimensional fluid element, thus implying that the particular fluid property are taken to be the same for the liquid- and gas- phases. Simply stated, the homogenous two-phase flow model thus transforms a real fluid into a pseudo fluid in an attempt to calculate fluid properties along the defined geometry.

This implies that the homogenous two-phase flow model does not account for velocity differentials that might occur between the liquid- and gas- phase, thus taking energy dissipation by inter phase friction to be negligible.

2.1.1 Gasifier Geometry and discretisation

The entire flow path is divided into a finite amount of elements that contains information describing amongst others geometrical properties like the physical inlet- and outlet- height of the element, inlet- and outlet- hydraulic diameter, cross sectional flow areas, the element length, the total secondary loss coefficient, average wall temperature, wall roughness coefficient, number of apertures applicable to the different concepts, as well as the diameter of the particular array of apertures applicable to the particular element.

2.1.2 Homogenous two-phase fluid properties

The effective fluid properties are defined in terms of the weighted average liquid- and gas-properties that are calculated as indicated in Eq. (2.1):

$$\frac{1}{\phi} = \frac{1-x}{\phi_L} + \frac{x}{\phi_G} \tag{2.1}$$

with ϕ representing any fluid property that might include the density, viscosity or conductivity applicable to the saturated liquid phase ϕ_L or saturated gas phase ϕ_G of the particular fluid. The quantity of the gaseous phase of the fluid present in the particular element are represented by x, with $0 \geq x \leq 1$ and $x = 0$ representing the liquid phase only, and $x = 1$ representing the presence of only the vapour phase at that point of the geometry. Thus, a fluid property is therefore described by a singular value applicable to the entire perimeter and length of the discretised element.

2.2 CONSERVATION EQUATIONS

The basic Gasifier geometry is reduced to a schematic as shown in Figure 2.1, and portrays the definition and nomenclature used for describing the flow by natural convection through the sub-elements of the Gasifier.

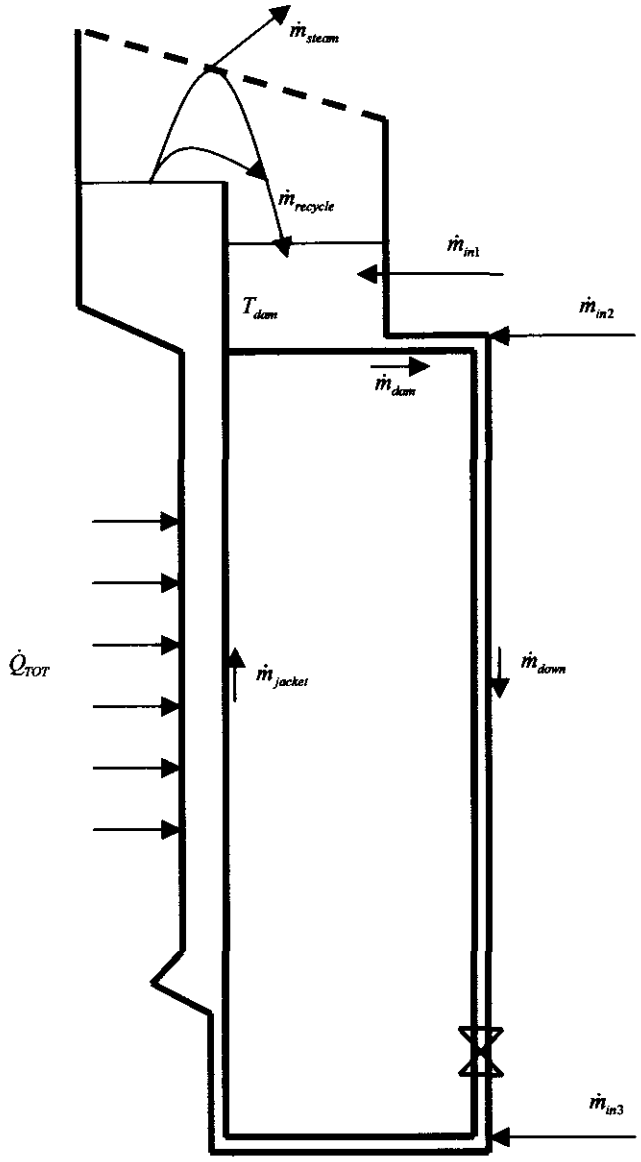

Figure 2.1: Schematic representation of the basic layout showing the definition and nomenclature used for indicating mass flow in the different sub-elements of the Gasifier.

2.2.1 Mass Conservation Equations

Total heat transfer rate from the inside of the Gasifier wall to the cooling jacket is depicted by $\dot{Q}_{TOT}$. The steady state fluid temperature in the top of the Gasifier is represented by T_{dam}, and the boiler feed water temperature T_{in} is taken to be $105^{\circ}C$ for all the different down comer configurations to be simulated. The total mass flow rate leaving the dam from the top of the Gasifier convected by the down comers to the Gasifier bottom are denoted by $\dot{m}_{dam}$.

The divided mass flow rate in each down comer is denoted by $\dot{m}_{down}$ with the mass flow rate through the Gasifier water jacket symbolised by $\dot{m}_{jacket}$. The mass flow rate of steam leaving the Gasifier top is depicted by $\dot{m}_{steam}$ and used downstream for process heating purposes. The amount of fluid returning to the dam in the Gasifier top to be re-circulated through the cycle is represented by $\dot{m}_{recycle}$ and is equal to the sum of liquid flowing over the wall of dam B into dam A plus the saturated liquid that have condensed on the screen positioned at the Gasifier outlet.

The mass flow rate of boiler feed water entering the Gasifier via three inlet ports in dam A at the Gasifier top are depicted by $\dot{m}_{1..3}$.

The various boiler feed water inlet position configurations investigated as disclosed are simulated by setting the indicated parameters as shown in Eq. (2.2) to Eq. (2.5):

- Configuration 1: $\dot{m}_{in1} = \dot{m}_{steam}, \dot{m}_{in2} = 0, \dot{m}_{in3} = 0, \dot{m}_{down} > 0.$ (2.2)
- Configuration 2: $\dot{m}_{in1} = 0, \dot{m}_{in2} = \dot{m}_{steam}, \dot{m}_{in3} = 0, \dot{m}_{down} > 0.$ (2.3)
- Configuration 3a: $\dot{m}_{in1} = 0, \dot{m}_{in2} = 0, \dot{m}_{in3} = \dot{m}_{steam}, \dot{m}_{down} > 0.$ (2.4)
- Configuration 3b: $\dot{m}_{in1} = 0, \dot{m}_{in2} = 0, \dot{m}_{in3} = \dot{m}_{steam}, \dot{m}_{down} = 0.$ (2.5)

It is assumed that all of the saturated steam produced in the Gasifier jacket minus the amount of condensate that formed on the perforated cone at the steam outlet of the Gasifier is fed to the inlet of the Gasifier jacket through the down comers. Thus the mass flow rate of steam to the Gasifier can be calculated as indicated in Eq. (2.6).

$$\dot{m}_{steam} = \dot{m}_{jacket}\, x_n \left(1 - f_{cond}\right) \tag{2.6}$$

The fraction of steam condensate is depicted by f_{cond} on the perforated cone at the outlet of the Gasifier with x_n representing the quality in the last element namely dam B. The influence of the rate of condensation (f_{cond}) on simulation results were analysed by substituting values of 5 %, 10 %, 15% and 20 %. Results revealed a negligible influence of the latter parameter, and a constant reference condensation rate of 10 % was used to conduct investigations of the different Gasifier water jacket geometries and boiler feed water inlet configurations.

The mass flow rate at which saturated liquid is returned to dam A is calculated as indicated in the Eq. (2.7).

$$\dot{m}_{recycle} = \dot{m}_{jacket} - \dot{m}_{steam} \tag{2.7}$$

From Figure 2.1, the mass balance for dam A can be calculated as shown in Eq. (2.8):

$$\dot{m}_{dam} = \dot{m}_{recycle} + \dot{m}_{in1} \tag{2.8}$$

The amount of liquid flowing through the down comers into the Gasifier water jacket is calculated by means of Eq. (2.9):

$$\dot{m}_{downm} = \dot{m}_{dam} + \dot{m}_{in2} \tag{2.9}$$

2.2.2 Momentum Conservation Equations

The one-dimensional steady state momentum conservation equation for each of the discretised elements can be written as indicated in Eq. (2.10).

$$p_{oe,i} = p_{oi,i} + \rho_i g\left(z_{i,i} - z_{e,i}\right) - \Delta p_{o,i} \tag{2.10}$$

The second subscript, i in each of the variable subscripts refers to the number of the particular element under consideration, p_{oi} and p_{oe} are the inlet- and outlet- total pressures respectively, z_i and z_e depicts the inlet- and outlet- elevations of the element. Gravitational acceleration is depicted by g and Δp_o represents the total pressure loss due to friction and other secondary pressure losses.

It is important to realise that if the elevation terms were included in the definition of total pressure as is usually the case, it would not be possible to simulate the flow by natural convection through the water jacket of the Gasifier.

2.2.3 Energy conservation Equations

The one-dimensional steady-state energy conservation for each element can be written as shown in Eq. (2.11),

$$\dot{m}_i h_{oe,i} = \dot{m}_i \left[h_{oi,i} + g\left(z_{i,i} - z_{e,i}\right) \right] + \dot{Q}_{H,i} \tag{2.11}$$

with $\dot{m}$ representing the mass flow rate, h_{oi} and h_{oe} the inlet and outlet total specific enthalpies respectively and $\dot{Q}_H$ the heat transfer rate to the fluid in element i.

The energy balance for the mixing taking place in dam A as shown in Figure 2.1, can be written as shown in Eq.

$$\dot{m}_{dam} h_{dam} = \dot{m}_{in1} h_{in1} + \dot{m}_{recycle} h_L\big|_{p=30.4\,bar} \tag{2.12}$$

with h_{dam} the enthalpy of the liquid leaving dam A, h_{in1} the enthalpy of the boiler feed water entering the dam, and $h_L\big|_{p=30.4\,bar}$ the enthalpy of saturated liquid at the system pressure of 30.4 bar.

2.3 CLOSURE EQUATIONS

Closure equations refer to the boundary values, state equations, heat transfer and pressure-drop correlations used in the simulation. Each of these will be discussed in the latter of this chapter.

2.3.1 Boundary conditions

The boundary conditions for this problem consist of the system pressure, which is equal to 30.4 bar, the boiler feed water temperature that is 105 °C and the Gasifier wall temperature distribution. This temperature distribution was obtained from measurements conducted by SASTECH and is shown as a function of elevation in Figure 2.2.

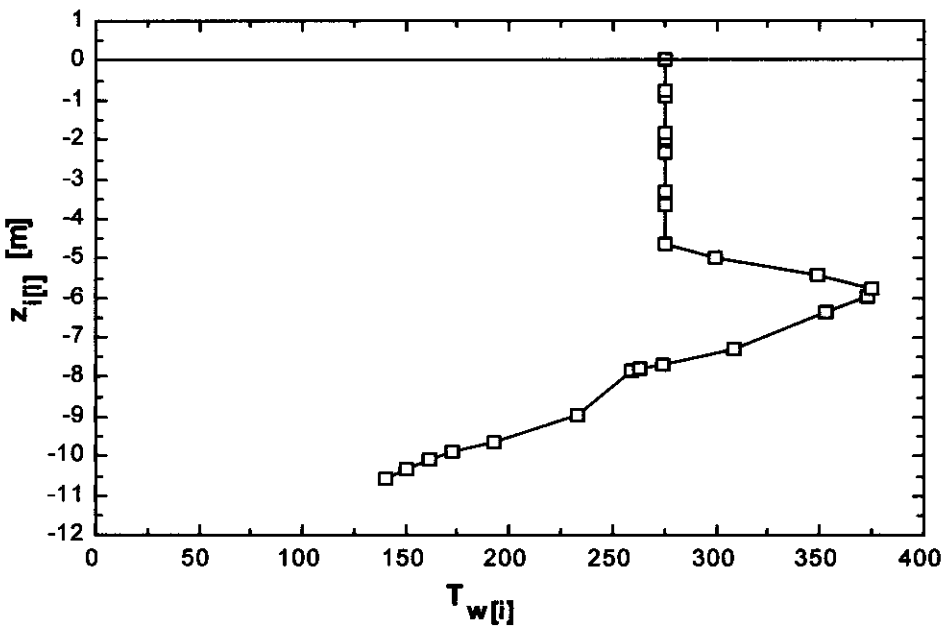

Figure 2.2: Gasifier wall temperature distribution versus elevation in the cooling jacket.

2.3.2 State Equations

The state equations for this simulation simply consist of the properties of water/steam mixtures. The models used for this are those included in the EES software package for water.

2.3.3 One-dimensional Two-Phase Pressure Drop

Two principles simulation approaches exist in the modelling of a two-phase flow system, as indicated in Chapter 1. The homogeneous approach, as proposed by Owens *(1961)* assumes equal liquid- and vapour- velocities, and average fluid properties across the element under

consideration. This modelling approach is applicable for a fog spray flow pattern occurring at high void fractions according to Tong *(1967)*. Owens proved that his relations could predict the pressure drop data of Schrock and Grossman *(1959)* with an error margin ranging from 10 % to 35 %. The data were for pressures ranging between 64 psia and 381 psia. The latter pressure range does not include the operating pressure of the Gasifying system.

The second approach or slip model as proposed by Lockhart-Martinelli-Nelson *(1948)* is applicable for annular flow patterns at intermediate void fractions. Colier and Hewitt *(1961)* along with Wicks, Dukler and Cleveland *(1964)* showed that the correlation of Martenelli et al. is as reliable as any annular flow pressure drop correlation available in the literature. For the purposes of evaluating fluid properties at different positions in the Gasifier convection cycle the latter proves to be more applicable due to the physical characteristics of water under high pressure- and temperature conditions. Therefore the approach and formulations to calculate pressure drop in the Lockhart-Martenelli-Nelson model will be implemented for the purposes of this study.

2.3.3.1 Lockhart-Martenelli-Nelson Two Phase Pressure drop

The Lockhart-Martenelli-Nelson model expresses two-phase pressure drop as a function of the pressure drop applicable to single phase vapour flow and a empirical correction factor ϕ_{gtt} as shown in Eq. (2.13),

$$\left(\frac{\Delta p}{\Delta l}\right)_{tpf} = \left(\frac{\Delta p}{\Delta l}\right)_{gpf} \phi_{gtt}^2 \tag{2.13}$$

where the subscript $_{tt}$, refers to turbulent gas flow, and turbulent liquid flow.

The equation describes the two-phase frictional pressure drop per unit length of duct as a function of the pressure drop experienced by the pressure loss due to friction of the gas phase alone, and ϕ_{gtt}^2 is an empirical function of X_{tt} as shown in Figure 2.3.

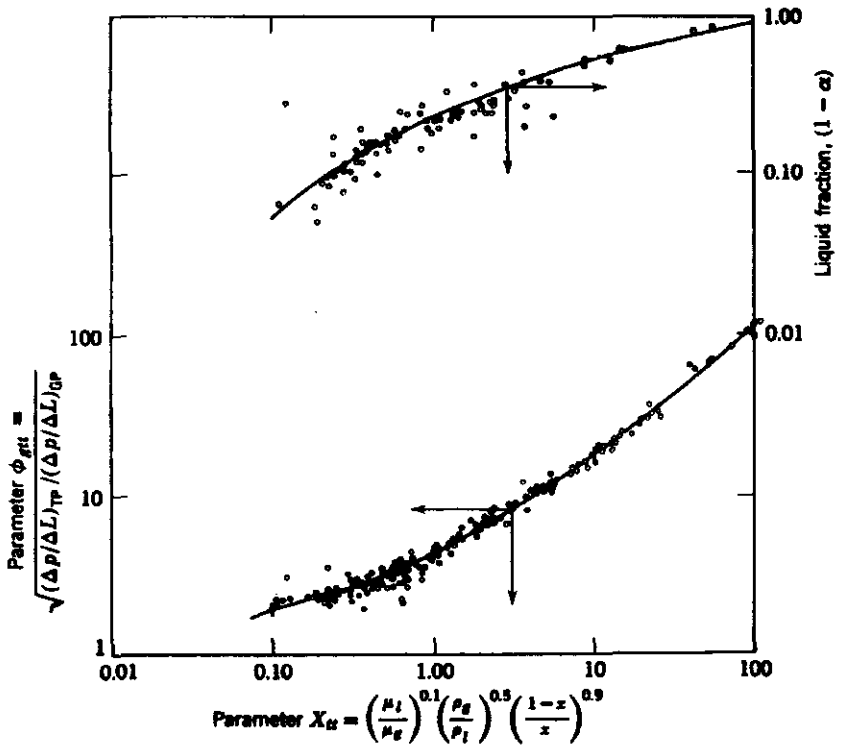

Figure 2.3: Relation between R_l, ϕ_{gg}; and parameter X for turbulent-turbulent flow, from Tong *(1967)*

An approximation of the measured data, represented by the solid line on the bottom of Figure 2.3 by means of curve fitting expresses ϕ_{gtt} as a function of X_{tt}, a dimensionless correlation parameter, is shown in Eq. (2.14):

$$\log\left(\phi_{gtt}\right) = 0.0948\left(\log\left(X_{tt}\right)\right)^2 + 0.5042\left(\log\left(X_{tt}\right)\right) + 0.6371 \tag{2.14}$$

As indicated in Figure 2.3, the dimensionless correlation parameter X_{tt}, obtained from dimensional analysis is calculated by implementing Eq. (2.15):

$$X_{tt} = \left(\frac{1-x}{x}\right)^{0.9}\left(\frac{\rho_g}{\rho_l}\right)^{0.5}\left(\frac{\mu_l}{\mu_g}\right)^{0.1} \tag{2.15}$$

with ρ_g and ρ_l depicting the density of the gas- and liquid phase of the fluid respectively. The liquid- and gas- phase viscosity of the fluid is represented by μ_l and μ_g respectively.

The friction factor for the calculation of the theoretical pressure drop for a single-phase flow is calculated by implementing the theory as proposed by Moody *(1944)*. An empirical formulation for determining the primary loss coefficient f accounting for pressure loss due to wall friction is given in Eq. (2.16):

$$f = \frac{0.25}{\left[\log\left(\frac{e}{3.7D} + \frac{5.74}{\mathrm{Re}^{0.9}}\right)\right]^2} \tag{2.16}$$

with e depicting the wall roughness coefficient ($e = 0.0005$, for mild steel), D represents the hydraulic diameter and Re represents the Reynolds number calculated by means the equation shown below.

$$\mathrm{Re} = \frac{\dot{m}x}{\rho_s A} \tag{2.17}$$

The mass flow of the pseudo fluid are represented by $\dot{m}$, x depicts the fluid quality with $0 \geq x \leq 1$, ρ_s are taken to be the density of the liquid phase if $x = 0$ and assumes the value of the density of the gaseous phase if $0 \geq x \leq 1$. The cross sectional area of the duct is depicted by A.

The two-phase pressure drop for each individual element is then calculated by means of Eq. (2.18),

$$\Delta P_{TP} = \frac{1}{2}\rho_g \left(f\frac{L}{D} + \sum K \right) V^2 \phi_{gtt}^2 \tag{2.18}$$

with K denoting secondary loss coefficients as applicable to the geometry of the flow path.

Clearly from the above the main pivot of the Lockhart-Martinelli-Nelson pressure drop calculation corrects the pressure drop of the gaseous phase present in the duct by implementing the correction factor ϕ_{gtt}.

As mentioned in the previous chapter, holes are drilled in the webs of the stiffening section in an effort to minimise the induced pressure drop across these sections.

The empirical correlation based on the work of Murdock was implemented to calculate the two-phase pressure drop of the fluid. The single-phase pressure drop can be readily calculated and the quality of the fluid through each element is known.

Test work by Murdock included the two-phase flows of steam-water, natural gas and water, natural gas-salt water, and natural gas-distillate combinations. His work includes three different test series for orifices equipped with radius, flange and pipe tap locations in 50 mm, 75 mm and 100 mm ID pipes, with orifice to pipe diameter pipe ratios ranging from 0.25 to 0.50. Pressures under which test work was conducted ranges from atmospheric pressure to 6.343 MPa, differential pressure from 0 to 124.42 kPa and liquid mass fractions from 2 % to 89 %. The temperature test range varied from $10^{\circ}C$ to 260° and varying Reynolds numbers ranging from 50 to 50 000 for the liquid phase and 15 000 to 1 000 000 for the vapour phase of the fluid.

The indicated ranges for the various fluid properties makes the theory of Murdock particularly applicable and therefore the pressure drop through the apertures (ΔP_{orr}) contained in the different belt jacket configurations can be calculated by implementing the following equation.

$$\Delta P_{orr} = \Delta p_g \left[1.26 \left(\frac{\Delta p_l}{\Delta p_g} \right)^{0.5} + 1 \right]^2 \tag{2.19}$$

The pressure drop (Δp_s) experienced by the respective liquid- and gas- phases are calculated by using the following:

$$\Delta p_s = \frac{1}{2Cd^2} \rho_s V_s^2 \tag{2.20}$$

The discharge coefficient (Cd) are taken to be equal to 0.6 which is applicable to sharp edged apertures; Δp_s, ρ_s and V_s represents the pressure drop, density and velocity for the liquid- and gas- phases of the fluid respectively. The velocities for the respective phases are calculated by using the following formulae:

$$V_l = (1-x)\frac{\dot{m}}{\rho_l A} \tag{2.21}$$

and

$$V_g = (x)\frac{\dot{m}}{\rho_g A} \tag{2.22}$$

2.3.4 *Two-phase Heat Transfer Equations*

2.3.4.1 Boiling regimes

The presence of both the liquid and vapour phase in this particular industrial problem occurs solely due to boiling, i.e. liquid evaporation occurs at the solid liquid interface. The collective term for this particular case of boiling is termed *pool boiling* due to the fact that the liquid remains quiescent and its motion near the heat transfer surface is due to free convection and to mixing induced by bubble growth and detachment. Boiling may also be classified according to whether it is sub-cooled or saturated. In sub-cooled boiling the temperature of the liquid is below the saturation temperature of the fluid and bubbles formed at the surface may condense and return to the liquid phase. However, if the temperature of the liquid slightly exceeds the saturation temperature, (with the difference between the surface and fluid temperature termed the excess temperature, $\Delta T_e \equiv T_s - T_{sat}$), saturated boiling occurs. This gave rise to extensive work done by Nukiyama, which found that different boiling regimes are encountered under different excess temperatures. This experimental investigation by Nukiyama gave rise to the so-called boiling curve for pool boiling. The boiling curve for water at atmospheric pressure is shown in Figure 2.4.

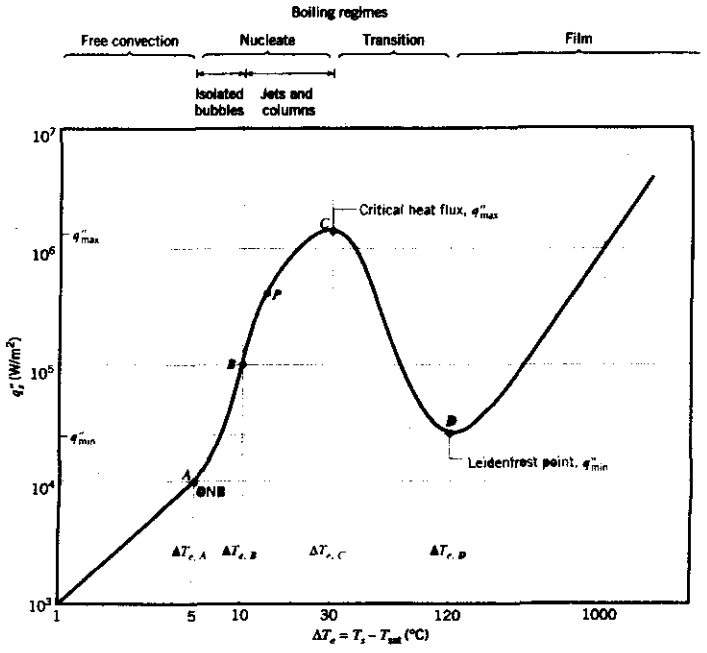

Figure 2.4: Typical boiling curve for water at atmospheric pressure: surface heat flux q''_s as a function of the excess temperature, $\Delta T_e \equiv T_s - T_{sat}$.

As shown in Figure 2.4, four different pool-boiling regimes are differentiated and are a function of the excess temperature. These four boiling regimes are defined as boiling by free convection, nucleate boiling, transition boiling and lastly film boiling.

2.3.4.1.1 Free Convection Boiling

Nukiyama found that free convection boiling exists if $\Delta T_e \leq \Delta T_{e,A}$ where $\Delta T_{e,A} \approx 5^{\circ}C$. In this regime, insufficient vapour is in contact with the liquid phase to cause boiling at the saturation temperature. A further increase in the excess temperature will cause bubble inception up to point A as shown in Figure 2.4, and is defined as the Onset of Nucleate Boiling (ONB). Free convection effects principally influence fluid motion.

2.3.4.1.2 Nucleate Boiling

Nucleate boiling exists in the range $\Delta T_{e,A} \leq \Delta T_e \leq \Delta T_{e,C}$ where $\Delta T_{e,C} \approx 30^{\circ}C$. In this range two different flow regimes are distinguished from another. As shown in Figure 2.4, the region depicted by A-B, isolated bubbles form at nucleation sites and separate from the surface, and induces considerable fluid mixing near to the fluid surface along with a considerable increase in the heat transfer coefficient h and $q_s^{"}$. Heat exchange takes place through direct transfer from the surface to the liquid in motion at the surface, and not via vapour bubbles rising from the heated surface.

As ΔT_e increases beyond $\Delta T_{e,B}$, more nucleation sites become active and increased bubble formation causes bubble interference and coalescence. In the region *B-C* vapour escapes as jets or columns, and subsequently merge into slugs of vapour.

This condition is illustrated in Figure 2.5, and shows that interference between the densely populated bubbles inhibits fluid motion near the heated surface. Point *P* in Figure 2.4 corresponds to an inflection point in the boiling curve, at which the heat transfer coefficient is a maximum. A further increase of ΔT_e from this point onwards results in a subsequent decrease in the heat transfer coefficient (h).

The surface heat flux $q_s^{"}$, however still increase which is the product of h and ΔT_e. The relative increase in ΔT_e exceeds the relative reduction in h for $\Delta T_e > \Delta T_{e,P}$, explaining the consequential

rise in $q_s^{"}$. Point C depicts the critical heat flux $q_{\max}^{"}$, the relative increase in ΔT_e is balanced by the reduction in the heat transfer coefficient h. The critical heat flux for water at atmospheric pressure exceeds $1\,MW/m^2$.

Considerable liquid vapour is formed at this point, restricting the heat transfer surface to be continually wetted. High heat transfer rates and heat convection coefficient are normally encountered in the nucleate boiling regime, necessitating engineering devices not to operate within these boundaries.

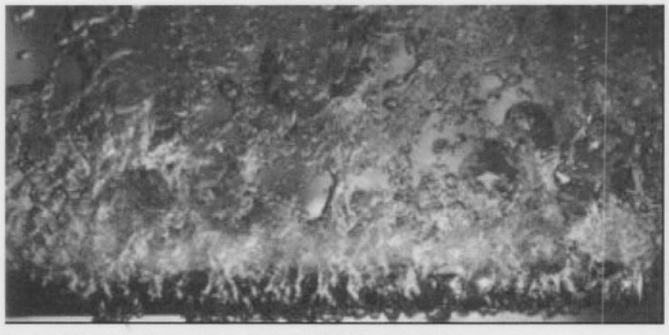

Figure 2.5: Nucleate boiling in the columns and jets regime.

2.3.4.1.3 Transition Boiling

As illustrated in Figure 2.4, the region corresponding to $\Delta T_{e,C} \le \Delta T_e \le \Delta T_{e,D}$ where $\Delta T_{e,D} \approx 120^{\circ}C$, and called transition boiling, unstable film boiling or partial film boiling. In this regime bubble formation is so rapid that a vapour or film blanket begins to form on the heated surface. Conditions may fluctuate between nucleate or film boiling on any point on the heated surface, but the fraction of heated surface covered by the film increases with increasing ΔT_e. The subsequent decrease in $q_s^{"}$ and h is ascribable to the thermal conductivity of the fluid vapour being considerably less than that of the liquid phase of the fluid with an increase in ΔT_e.

This phenomenon is illustrated in Figure 2.6.

Figure 2.6: Transition boiling

2.3.4.1.4 Film Boiling

This regime occurs for $\Delta T_e \geq \Delta T_{e,D}$, with point *D* depicted in Figure 2.4, the critical surface heat flux $q_s^{"}$ is a minimum and is called the Leidenfrost point. It was Leidenfrost that observed in 1756 that water droplets supported by the vapour film slowly boil away as the move about a hot surface. At this point, $q_{s,D}^{"} = q_{\min}^{"}$, a vapour blanket covers the total heat transfer surface.

From this point heat transfer occurs through conduction via the fluid vapour blanket. With a subsequent rise in surface temperature, radiation heat transfer starts to play a significant role and $q_s^{"}$ subsequently rise with a further increase in ΔT_e. Figure 2.7 shows the nature of vapour formation and bubble dynamics associated with film boiling.

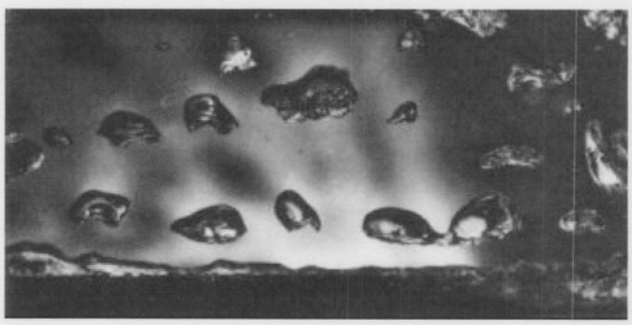

Figure 2.7: Film boiling

Many engineering applications i.e. heating devices require to be designed to operate in the region *A-C* as shown in Figure 2.5. By gradually increasing the surface heat flux by increasing the input power to the device, the excess temperature ΔT_e will increase as well as the heat transfer surface temperature T_s, following the boiling curve up to point *C*, the critical heat flux.

However, any further increase in the surface heat flux ($q_s^{"}$) beyond the critical heat flux will certainly induce a sharp deviation from the boiling curve in the event of which the surface conditions can change abruptly from $\Delta T_{e,C}$ to $\Delta T_{e,E} \equiv T_{s,E} - T_{sat}$. $T_{s,E}$ may exceed the heat transfer surface melting point with consequential failure or even destruction of the device. For this reason, point *C* is often referred to as the burnout point or the boiling crisis, and accurate knowledge at which point the critical heat flux (CHF) occurs is essential ($q_{s,C}^{"} \equiv q_{max}^{"}$), and the onset of the boiling crisis is shown in Figure 2.8.

The heat transfer area is preferably operated as close as possible to this point, with all design efforts made to ensure that this point is not exceeded.

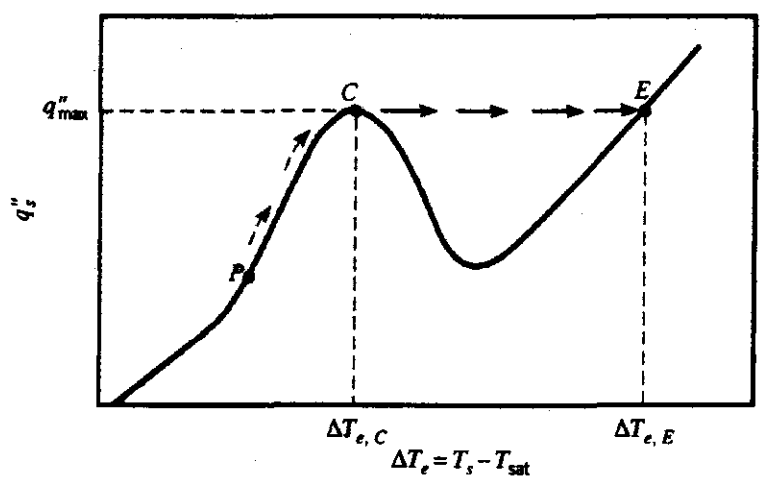

Figure 2.8: Onset of the boiling crisis.

The 65 mm thick inner wall of the Gasifier failed or bulged due to local hot spots forming due to the onset of the boiling crisis. Although the melting point of the metal wall was never reached, surface temperatures rose to the extent that diffusion of carbon to the grain boundaries caused 30 mm deep cracks in a pattern resembling that of an elephant's skin. The purpose of this study is thus also showing out these areas affected by the onset of the boiling crisis.

2.3.4.2 Implementation of Heat Transfer correlations

Although the simulation model incorporates theory accounting for heat transfer from the Gasifier wall to the water jacket, it does not account for energy losses to atmosphere due to the fact that the outer wall of the water jacket are thermally lagged and clad.

The Nusselt number provides a measure of the convection heat transfer occurring at the heat transfer surface. Three different scenarios applicable to the Nusselt number for the three fundamental flow conditions that might occur in any flow, namely laminar flow, transitional flow and turbulent flow are distinguished in the model.

- **Laminar flow condition** ($\mathrm{Re} < \mathrm{Re}_{lam} = 2200$):

  Therefore, the above assumption allows the implementation of the theory of Rosenhow *(1952)* applicable for fully developed velocity profiles and isothermal walls as shown in Eq. (2.23):

$$Nu_{lam} = 3.656 \tag{2.23}$$

  where Nu_{lam} represents the Nusselt number for the laminar flow regime.

- **Transitional flow regime** ($\mathrm{Re}_{lam} < \mathrm{Re} < \mathrm{Re}_{tur}$):

  In the transition range the following cubic interpolation as proposed by Stempniewicz ensures a smooth transition from the laminar to turbulent regions, as shown in Eq (2.24).

$$Nu_{tran} = Nu_{lam} - \left(Nu_{lam} - Nu_{tur}\right)\left(3 - 2\left(\frac{\mathrm{Re} - \mathrm{Re}_{lam}}{\mathrm{Re}_{tur} - \mathrm{Re}_{lam}}\right)\right)\left(\frac{\mathrm{Re} - \mathrm{Re}_{lam}}{\mathrm{Re}_{tur} - \mathrm{Re}_{lam}}\right)^2 \tag{2.24}$$

Nu_{tran} depicts the Nusselt number in the Transitional flow regime, Nu_{tur} depicts the Nusselt number in the turbulent flow regime, Re_{lam} represents the Reynolds number in the laminar flow regime and Re_{tur} depicts the Reynolds number in the turbulent flow regime.

- **Turbulent flow regime** ($\mathrm{Re} > \mathrm{Re}_{tur} = 10000$):

  The Dittus-Boelter *(1930)* equation are applied in the turbulent flow regime,

$$Nu_{tur} = 0.23\,\mathrm{Re}^{0.8}\,\mathrm{Pr}^{0.4} \tag{2.25}$$

where the Prandtl number is represented by Pr and calculated using the following relation,

$$\mathrm{Pr} = \frac{c_p \mu}{k} \tag{2.26}$$

with c_p representing the specific heat coefficient under constant pressure, thermal conductivity represented by k and μ depicts the kinematic viscosity of the fluid.

2.3.4.2.1 Equations for free convection heat transfer

Heat transfer by natural convection for the fluid in the liquid phase only is calculated by means of the following equation.

$$Q = hA_h\left(T_w - T\right) \tag{2.27}$$

with the heat transfer coefficient depicted by h, the heat transfer area is represented by A_h, T_w depicts the wall temperature as specified in the boundary conditions, and the fluid temperature in the element is represented by T.

It must be noted that substitution of the Nusselt number described by Rosenhow eliminates the unknown heat transfer coefficient for the particular, and therefore the heat transfer by natural convection for the instance where only the liquid phase are encountered in a particular element can be calculated by:

$$Q = Nu\frac{k}{D}A_h\left(T_w - T\right) \tag{2.28}$$

where D depicts the hydraulic diameter of the particular element.

2.3.4.2.2 Equations for nucleate boiling

Two correlations are available for the nucleate pool boiling regime namely theory developed by Rosenhow *(1952)* and Chen *(1963)*. The correlation of Chen is applicable to internal flow surface, i.e. inside surfaces of cylindrical and spherical geometry. The correlation of Rosenhow however, is applicable to external flow, i.e. outside surfaces of cylindrical and spherical geometry. Heat flux by nucleate boiling in the instance of the Gasifier water jacket is calculated by implementing the correlation of Rosenhow as shown below,

$$q_{nuc} = \mu_L h_{LG}\left(\sqrt{\left[\frac{g\left(\rho_L - \rho_G\right)}{\varepsilon}\right]}\right)\left(\frac{c_{p,L}\left(T_w - T\right)}{C_{sf}h_{LG}\,\mathrm{Pr}_L}\right)^3 \tag{2.29}$$

with q_{nuc} representing the heat flux, μ_L being the viscosity of the liquid phase at the mean fluid temperature, h_{LG} signifies the latent heat of evaporation for the fluid, $c_{p,L}$ denotes the specific heat of the liquid phase, T symbolizes the average of the inlet- and outlet- fluid temperature, C_{sf} signifies a constant dependant on the heat transfer surface and fluid type ($C_{sf} = 0.0068$; for water and scored metal), Pr_L denotes the Prandtl number as calculated for the liquid phase, g symbolizes the gravitational acceleration constant, ρ_L and ρ_G denotes the liquid- and vapour-phase densities respectively and ε denotes the surface tension of the fluid at T.

Two models describe the critical heat flux as discussed in 2.3.4.1.4. The first are referred to as the pool boiling critical heat flux model and the second is known as the convective boiling critical

heat flux. The convective boiling model is applicable to internal flows with the pool-boiling model relevant to external flows.

The pool boiling critical heat flux model is based on the Zuber *(1959)* correlation, including the Ivey-Morris *(1962)* correction factor C_{I-M} for sub-cooling, geometry dependant constant C_{geom} as well as a quality dependant multiplier. The critical heat flux is calculated by means of the following formula.

$$q_{CHF} = q_{zub} C_{I-M} C_{geom} (1-x) \tag{2.30}$$

with

$$C_{I-M} = 1 + 0.1 \frac{\rho_L c_{p,L} (T_{sat} - T)}{\rho_G h_{LG}} \sqrt[4]{\frac{\rho_G}{\rho_L}} \approx 1 \tag{2.31}$$

The values of the geometry dependant multiplier C_{geom}, are based on the extension of the Zuber theory by Leinhard *(1973)*, Sun *(1970)*, and Ded *(1972)*. Due to the large diameter of the Gasifier, the circumference thereof can be approximated by a flat plate. Therefore, the geometry dependant multiplier C_{geom} is set to a value of 1.140.

As indicated in the previous paragraph, fluid flow in the Gasifier water cooling jacket is of external flow nature, making the pool boiling critical heat flux model applicable. The Zuber correlation is implemented to calculate the critical heat flux as shown in the following equation.

$$q_{zub} = \left[C_{zub} h_{LG} \rho_G \sqrt[4]{\left(\frac{\varepsilon g (\rho_L - \rho_G)}{\rho_G^2} \right)} \sqrt{\frac{\rho_L + \rho_G}{\rho_L}} \right] \cdot 1 \cdot 1.14 (1-x) \tag{2.32}$$

The value of constant C_{zub} is set to 0.18, which agrees better with the originally proposed value of 0.13 as proposed by Zuber (see Rosenhow *(1973)*).

It is important to note that the critical heat flux is strongly dependant on pressure, mainly through the pressure dependence of surface tension and the heat of vaporization. Cichelli and Bonilla *(1945)* have experimentally demonstrated that the peak heat flux increases with pressure up to one-third of the critical pressure, after which it falls to zero at the critical pressure.

If $T_w < T_{CHF}$, the total heat transfer by means of nucleate boiling is calculated by,

$$Q_{nuq} = q_{nuc} A_h \tag{2.33}$$

where A_h depicts the total heat transfer area applicable to the element.

2.3.4.2.3 Equations for film boiling

As indicated in paragraph 2.3.4.1.4, two heat transfer mechanisms are present when film boiling persists, namely convective- and radiative- heat transfer. Therefore, the overall heat transfer coefficient must consist of the weighted sum of both the former and latter heat transfer coefficients. The convective heat transfer coefficient is calculated for pool conditions, with the radiation heat transfer coefficient calculated implementing the black body radiation law.

Collier postulated that the overall heat transfer coefficient in the film-boiling regime could be calculated by implementing the following relationship,

$$h = h_{conv} + 0.75 h_{rad} \tag{2.34}$$

where h_{conv} and h_{rad} depicts the convective- and radiative heat transfer coefficients respectively.

The convective heat transfer coefficient is calculated as indicated by Stempniewicz,

$$h_{conv} = C\sqrt[4]{\frac{k_G^3 \rho_G g(\rho_L - \rho_G)(h_{LG} + 0.4c_{p,G}(T_w - T_{sat}))}{\mu_G D_o (T_w - T_{sat})}} \tag{2.35}$$

where C represents a constant that is geometry dependant, k_G depicts the vapour thermal conductivity, and D_o denotes a characteristic geometry dependant dimension. In the case of the Gasifier $D_o = H$ as indicated by Bromley for vertical walls and $C = 0.625$.

For the radiative heat transfer coefficient, the black body radiation law is implemented, with the radiative heat flux being equal to,

$$q_{rad} = \sigma(T_w^4 - T_{sat}^4) \tag{2.36}$$

the radiative heat transfer is calculated from,

$$\begin{aligned} h_{rad} &= \frac{q_{rad}}{(T_w - T_{sat})} \\ &= \sigma(T_w + T_{sat})(T_w^2 + T_{sat}^2) \end{aligned} \tag{2.37}$$

and σ designates the Stefan-Boltzmann constant ($\sigma = 5.67 \times 10^{-8}$).

If $T_w > T_{CHF}$, the total heat transfer by means of film boiling is calculated by the following equation.

$$Q_{film} = q_{film} A_h \tag{2.38}$$

2.3.4.2.4 Equations for transition boiling

For the purpose of calculation the heat flux in the transition-boiling regime, the formulation proposed by Kalinin *(1975)* is implemented as indicated below.

$$q_{trans} = a_{wet} q_{CHF} + a_{dry} q_{MFB} \tag{2.39}$$

The critical heat flux is denoted by q_{CHF}, the heat flux at the point of minimum film boiling is represented by q_{MFB} and $a_{wet} + a_{dry} = 1$.

The parameter a_{dry} is calculated using the following formulation proposed by Kalinin,

$$a_{dry} = 1 - \left(\frac{\Delta T_{MFB} - \Delta T_w}{\Delta T_{MFB} - \Delta T_{CHF}} \right)^7 \tag{2.40}$$

with $\Delta T_{MFB} = T_{MFB} - T_{sat}$ depicting the wall superheat at the minimum film boiling point, $\Delta T_{CHF} = T_{CHF} - T_{sat}$ portrays the degree of superheat at the critical heat flux point and $\Delta T_w = T_w - T_{sat}$ represents the degree of superheat at the wall.

The parameter a_{wet} in the Kalinin correlation is calculated as indicated in the equation below.

$$a_{wet} = \left(\frac{T_{MFB} - T_w}{T_{MFB} - T_{CHF}} \right)^7 \tag{2.41}$$
$$\therefore a_{dry} = 1 - a_{wet}$$

The heat transfer coefficient in the transition-boiling regime is obtained from

$$h_{trans} = \frac{a_{wet} q_{CHF} + a_{dry} q_{MFB}}{T_w - T_{sat}} \tag{2.42}$$

Heat flux at minimum film boiling or the Leidenfrost point D as shown in Figure 2.4 is characterised by a transition from a partially wetted heating surface to a dry heating surface. Zuber as indicated below calculates the Leidenfrost point using another correlation.

$$q_{MFB} = 0.09\rho_G h_{LG}\left(\sqrt[4]{\frac{\sigma}{g(\rho_L-\rho_G)}}\right)\left(\sqrt{\frac{g(\rho_L-\rho_G)}{\rho_L+\rho_G}}\right) \tag{2.43}$$

The temperature at which the point of minimum film boiling occurs is calculated using the correlation of Simon *(1968)*.

$$T_{MFB} = T_{crit}\left(0.13\frac{p}{p_{crit}}+0.86\right) \tag{2.44}$$

The critical temperature of water as depicted by Reid *(1989)* is substituted as $T_{crit} = 647.3\ K = 374.15^{\circ}C$, and the critical pressure of water is taken as $p_{crit} = 2.212\times10^{7}\ Pa$.

If $T_{MFB} < T_w > T_{CHF}$, the total heat transfer by means of transition boiling is calculated by the following equation.

$$Q_{trans} = q_{trans}A_h \tag{2.45}$$

2.4 SUMMARY

This chapter outlined the theory and methodology for the implementation of a steady-state one-dimensional homogenous two-phase flow model. The model is written to calculate flow losses and heat transfer, based on measured jacket temperatures and boiler feed water inlet temperature and flow rate. The main assumption of homogenous two-phase flow is that fluid properties are assumed to be constant across any cross sectional area of the one-dimensional fluid element. Both the liquid and vapour phase velocity is assumed to be equal thus permitting no slip between the phases.

Mass conservation equations are derived that specifically describe the flow path in the Gasifier. A condensation rate was introduced to account for losses in steam production due to condensation on the conical screen before the Gasifier outlet. The different boiler feed water inlet configurations are incorporated in the derivation of the mass balance.

The derivation of the momentum conservation equation differs from the definition of total pressure. Natural convection driven flow through the Gasifier jacket requires the elevation terms to be excluded from the definition of total pressure.

The energy conservation equation takes the elevation of each of the elements into account. Furthermore, an equation was derived to account for mixing that takes place in dam A of the Gasifier.

Closure is given to the system of unknowns by means of the incorporation of the built in state equations as offered by EES. Pressure loss due to friction is incorporated, as is custom with single-phase flow systems. Apertures in the Stiffener ring geometries are included by means of secondary loss coefficients as applicable to orifices.

The heat transfer model for single phase flow is based on the Dittus-Boelter equations, while for the two-phase flow it takes into account the different boiling regimes. This includes the nucleate-, transition- and film-boiling regimes.

The next chapter considers measured results as obtained by SASTECH that will be used to verify the simulation model against.

2.5 REFERENCES

COLLIER, J.G. & HEWITT, G.F., 1961. Data on the Vertical Flow of Air-Water Mixtures in the Annular and Dispersed Flow regions, Part II: Film thickness and Entrainment Data and Analysis of Pressure Drop Measurements, Trans. Inst. Chem. Eng., Vol. 59, pp. 127-136.

COLLIER, J.G., 1981, Convective Boiling and Condensation, McGraw Hill, First edition: 1972, Second Edition: 1981.

CICHELLI, M.T. & BONILLA, C.F., 1945. Heat Transfer to Liquids Boiling Under Pressure. Trans. AIChE, **41**, p.755.

CHEN, J.C., 1963. A correlation for boiling heat transfer to saturated liquids in convective flow. ASME preprint 63-HT-34 presented at the 6th National Heat Transfer Conference, Boston, August 1963.

DITTUS, F.W. & BOELTER, L.M.K., 1930. Publications on Engineering, University of California, Berkerley, **2**, p. 443.

DUKLER, A.E., Wicks, M. & CLEVELAND, R.G., 1964. Frictional Pressure Drop in Two-Phase Flow; Part A, A comparison of Existing Correlations for Pressure Loss and Holdup, AIChE J., **10**(1), pp. 38-43.

DED, J.S. & LEINHARD, J.H. 1972. The peak Pool Boiling Heat Flux from a Sphere. AIChE J., **18**(2), p. 337.

HSU, Y.Y., GRAHAM, R.W., 1976, Transport process in Boiling and Two-Phase Systems, ISBN 0-07-030637-0, McGraw Hill.

INCROPERA, FRANK.P. & DE WITT, DAVID.P., 1996. Fundamentals of heat and mass transfer, USA: John Wiley & Sons, p. 546.

IVEY, H.J. & MORRIS, D.J., 1962. On the relevance of the Vapour-Liquid Exchange Mechanism for Sub-cooled Boiling Heat Transfer at High Pressure. UK Rept. AEEW-R-137, Winfrith.

KALININ, E.K., BERLIN, I.I., KOSTYUK, V.V., NOSOVA, E.M., 1975, Heat Transfer in Transition Boiling of Cryogenics, paper presented at Cry. Eng. Conf., Queens Univ. Kingston, Ontario, Canada, July.

LEINHARD, J.H., DHIR, V.K., 1973, The Extended Hydrodymic Theory of the Peak and Minimum Pool Boiling Heat Fluxes, NASA CR 2270.

LOCKHART, R.W., MARTENILLI, R.C., 1949, Proposed Correlation of Data for Isothermal Two-Phase Two-Component Flow in Pipes, Chem. Eng. Prog., **45**, p. 34-48.

MARTINELLI, R.C., NELSON, D.B., 1948, Prediction of Pressure Drop During Forced Circulation Boiling of Water, Trans. ASME, Vol. 66, p. 695.

MOODY, L.F., 1944. Friction factors for pipe flow. Trans. AMSE, Vol. 69, pp. 671-684.

ROSHENHOW, W.M., 1952, A Method of Correlating Heat Transfer Data for Surface Boiling of Liquids, Trans. ASME, **74**, p. 969.

ROSENHOW, W.M., 1973, Handbook of Heat Transfer, McGraw Hill Book Company, ISBN 0-07-053576-0, New York.

SIMON, F.F., PAPELL, S.S, SIMONEAU, 1968, R.J., Minimum Film Boiling Heat Flux in Vertical Flow of Liquid Nitrogen, NASA TND-4307.

SCHROCK, V.E. & GROSSMAN, L.M., 1959. Forced Convection Boiling Studies, U. of California Insy. Of Eng., Res. Rept. Ser. 73308-UCX 2182, No. 2.

STEMPNIEWICZ, M.M., 2000, Simulation of Containment Transient Response During Accidents in Advanced Reactor Types, Arnhem, May 12, pp. 160-172.

SUN, K.H. & LEINHARD, J.H., 1970. The Peak Pool Boiling Heat Flux on Horizontal Cylinders. Int. J. Heat and Mass Transfer, **13**(9), pp.1425-1439.

TONG, L.S., 1967, Boiling heat transfer and two-phase flow, USA: John Wiley & Sons. pp. 77-103.

ZUBER, N., TRIBUS, M., 1958, Further Remarks on the Stability of Boiling Heat Transfer, UCLA Rept. 58-5.

ZUBER, N., 1959, Hydrodynamic Aspects of Boiling Heat Transfer, USAEC Rept. AECU-4439; doctoral dissertation, university of California at Los Angeles.

CHAPTER 3: VERIFICATION OF THE STEADY STATE HOMOGENEOUS TWO-PHASE FLOW MODEL

3. Introduction

This chapter is dedicated to the verification of the steady state homogenous two-phase flow model. SASTECH, a division of SASOL, measured Flow rate and temperatures at various positions along the Gasifier geometry. Measurements where recorded over a period of nine consecutive days of operation, which included the initial start-up, steady state-operation and shutdown of the Gasifier.

The first section of this chapter reflects the measured data used for verification of the simulation model. The total system pressure was used as the main indicator to determine steady state operating conditions, as an adversely fluctuating system pressure does not reflect steady-state conditions. The standard deviation from the mean total system static pressure should therefore be as small as possible. Furthermore, the average system pressure must be as close to the system operating design pressure of 3040 kPa. A total of one hundred data points that conforms to these criteria are isolated and is discussed in this chapter. The average of the measured parameter, along with the mean deviation (where applicable) is calculated over the measured period.

The second section of the chapter presents the simulation results obtained for the Base case scenario, and includes the geometry of the un-modified Gasifier with down comer configuration one.

Measured averaged results are then compared with results as given by the simulation model. This is done to determine the overall accuracy of the simulation model in comparison with real flow in the Gasifier system.

3.1 PROCESS PARAMETER MEASUREMENTS

To enable the verification of the simulation model, the following measurements where taken.

- System total pressure measurement,
- Volume flow rate measurements in the three down-comers,
- Temperature measurement in dam A,
- Water temperature measurement at six different locations in the Gasifier jacket annulus at 0.5-meter intervals,
- Temperature measurements on the down comer skins at the dam outlet, mixed stream and bottom re-entry inlet temperatures,
- Boiler feed water mass flow rate, and
- Total steam production.

The process parameters listed above constitute the Key Performance indicators mentioned in the first chapter of this dissertation.

Flow rates where measured by means of *Vera-bars*, that measures the differential pressure across an obstruction placed within the flow path. A multiplication factor was used to compensate for the density of the flow to give mass flow. Temperature measurements where taken by installing thermocouples in contact with the fluid and the Gasifier inner walls. Due to the transient behavior of the Gasifier system, a high data resolution was chosen. Measured data was recorded and stored on 15-second intervals, and recorded over a period of nine days. The model however, does not take changes with time in consideration. Therefore acquired data for steady state Gasifier operation will be used for verification purposes.

Steady state operating conditions are determined from the system total pressure measurement data, i.e. total system pressure that is closest to the specified system operating pressure of 3040 kPa.

3.1.1 System Total Pressure Measurement

The system total pressure measurement is used as input to determine steady state Gasifier operating conditions. Figure 3.1 depicts the steady-state operating system total pressure measurement for the Gasifier for a hundred data points.

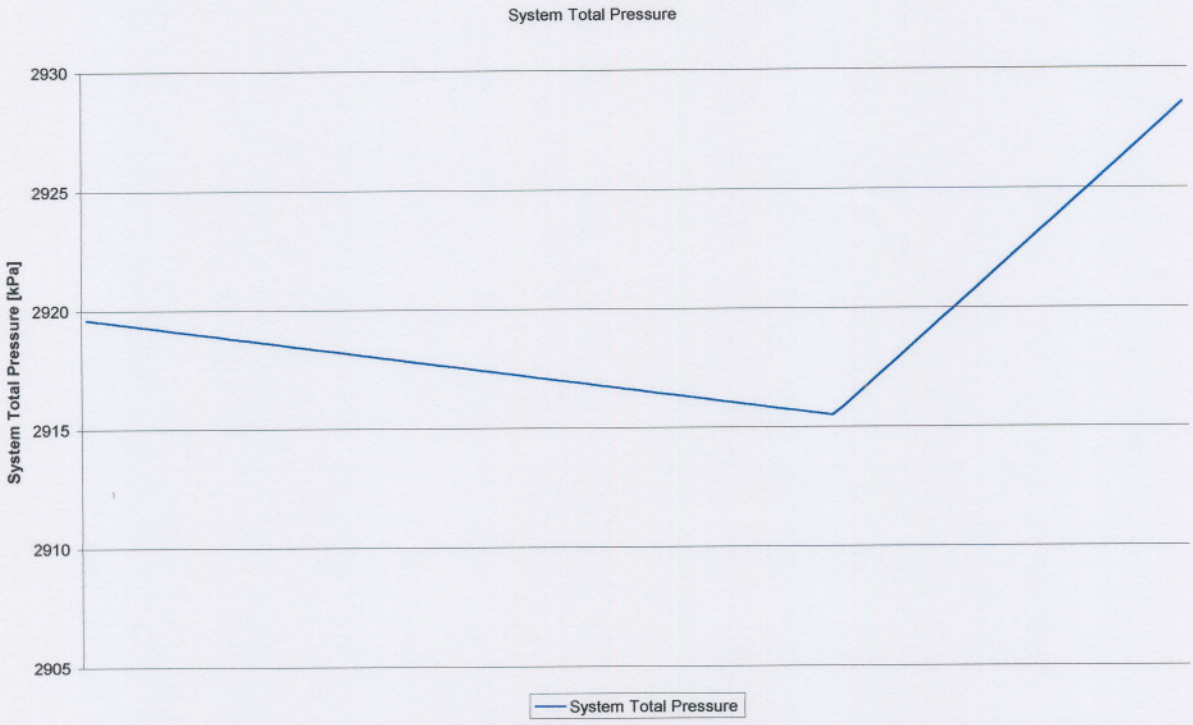

Figure 3.1: System total pressure measurements for steady state Gasifier operating conditions.

The average system pressure for this period was 2919.04 kPa, and is a good approximation of the specified 3040 kPa system operating pressure used in the model. The standard deviation for the data reflected in Figure 3.1 was calculated to be 3.2 %. The data measured for this period therefore satisfy the filtering criteria and the remainder of the data reflected in this chapter corresponds to the same time period.

3.1.2 *Volume Flow Rate Measurement in Down Comers*

The volume flow rate was measured separately for each of the three down comers and is shown in Figure 3.2.

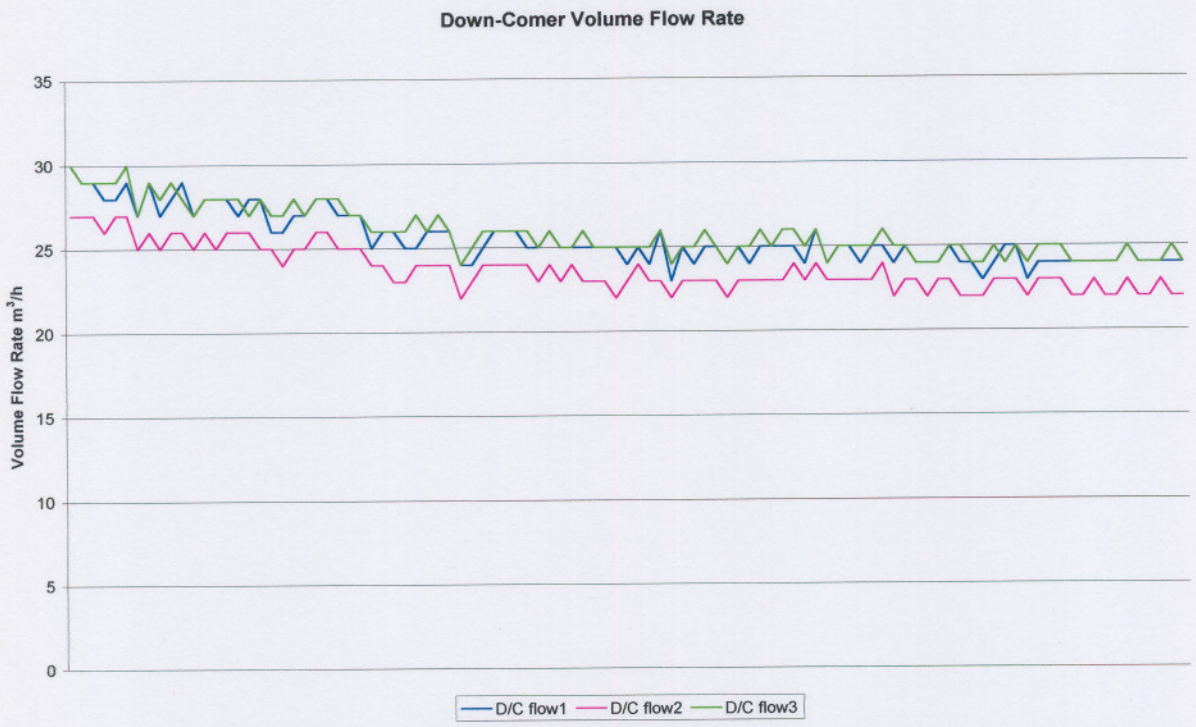

Figure 3.2: Volume flow rate in each of the three down comers for steady state Gasifier operating conditions.

The average volume flow rate measured for each of the down comers over the period corresponding to recorded measurements taken for the total static pressure is summarised in Table 3-1.

	Volume Flow Rate [m^3/h]
Down Comer 1	25.50
Down Comer 2	23.71
Down Comer 3	25.86
Average volume flow rate per down comer	**25.02**

Table 3-1: Average down comer volume flow rate measurement

3.1.3 *Temperature Measurement in dam A*

The temperature measured in dam A over the corresponding period is shown in Figure 3.3.

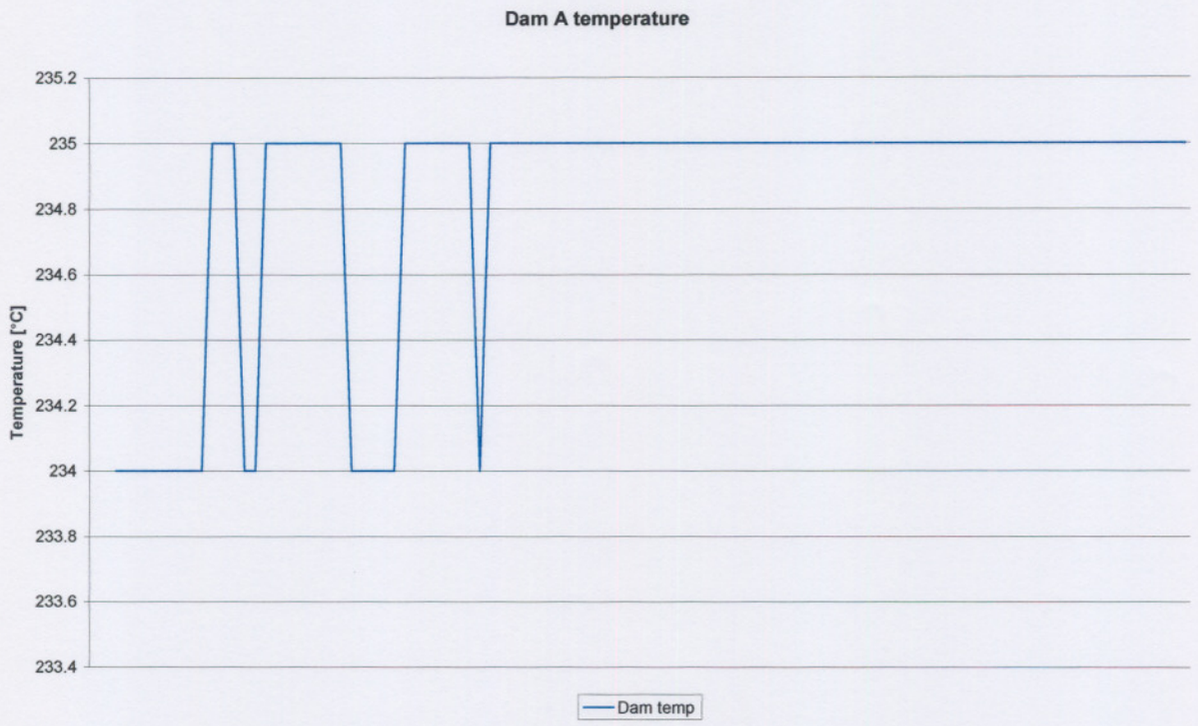

Figure 3.3: Temperature measurement in dam A for steady state Gasifier operation.

The average dam A temperature for the mentioned period of time was 234.83 °C. It is furthermore noted that the temperature does not vary more than 1 °C.

3.1.4 *Water temperature measurement in Gasifier Jacket annulus*

Water temperature measurements where taken at six different axial locations of the Gasifier. Temperatures reflected in Figure 3.4, were measured 5-mm from the outer jacket for the water annulus.

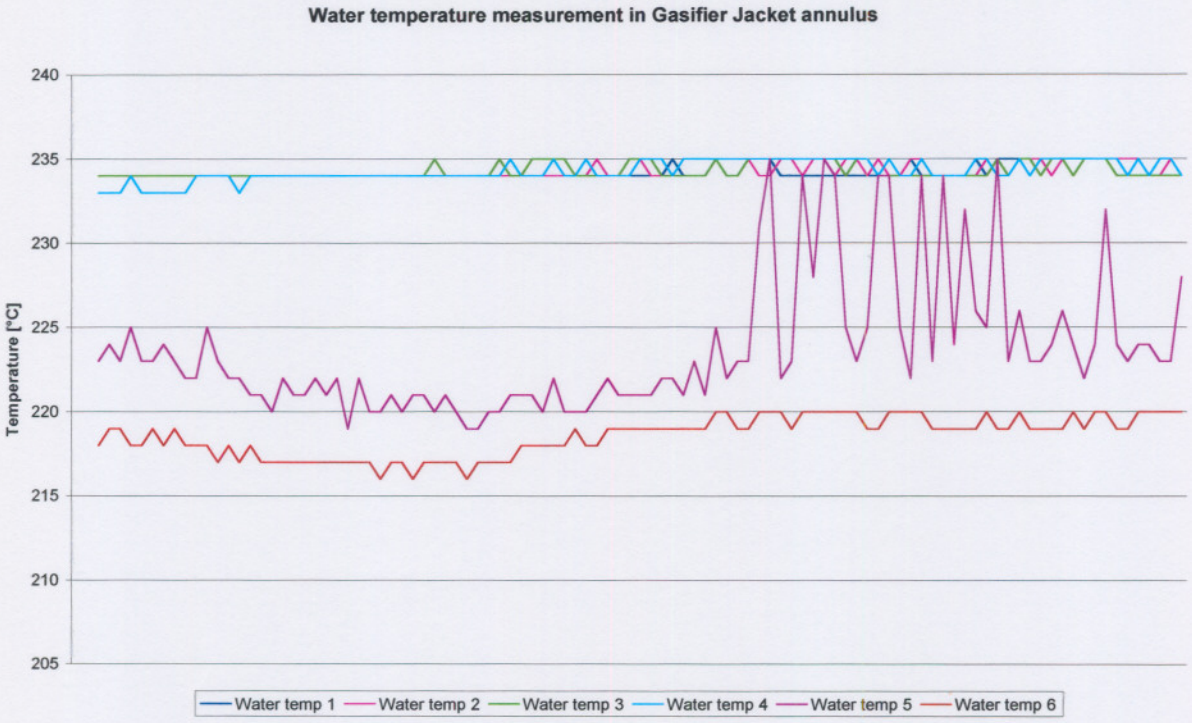

Figure 3.4: Water temperatures in the Gasifier annulus under steady state operation

Water temp 1 is at the raw gas outlet of the Gasifier, and *Water temp 6* positioned at the bottom of the Gasifier.

The average water temperatures for the six different locations are summarised in Table 3-2.

Position	[°C]
Water temp 1	234.19
Water temp 2	234.28
Water temp 3	234.29
Water temp 4	234.31
Water temp 5	223.67
Water temp 6	218.54

Table 3-2: Average water temperatures in the Gasifier water jacket annulus under steady state operation

3.1.5 Down Comer water temperature measurements

Temperatures in the down comers were measured on the pipe surfaces, at three different locations. The first skin thermocouple was placed to measure the water temperature, exiting dam A (D/C Feed Skin). The second skin thermo-couple measured the mixed water temperatures that consist of boiler feed water and water from dam A (D/C Top Temp). The third skin temperature measurement was taken at the point where water enters the bottom of the Gasifier from the down comer (D/C bottom temp). Nine measurement points where therefore installed on the three down comers, and is shown in

Figure 3.5.

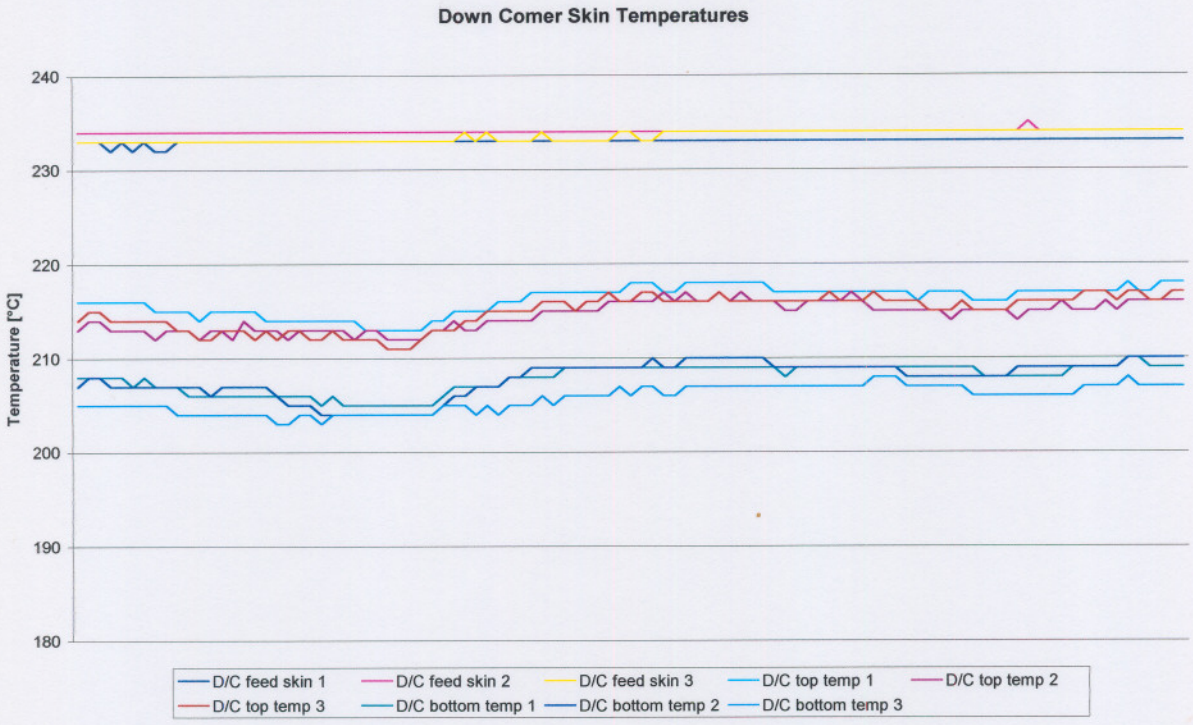

Figure 3.5: Down comer water temperature measurements for steady state Gasifier operation.

The average temperatures measured for the positions discussed is summarised in Table 3-3.

Position	[°C]
D/C feed skin 1	232.96
D/C feed skin 2	234.01
D/C feed skin 3	233.52
D/C top temp 1	216.15
D/C top temp 2	214.50
D/C top temp 3	214.86
D/C bottom temp 1	207.83
D/C bottom temp 2	207.83
D/C bottom temp 3	205.71

Table 3-3: Average down comer temperatures for steady state Gasifier operation.

3.1.6 *Total steam production and boiler feed water mass flow rate measurement*

The total steam production and boiler feed water flow rate was measured, and recorded data for steady state Gasifier operation is shown in Figure 3.6.

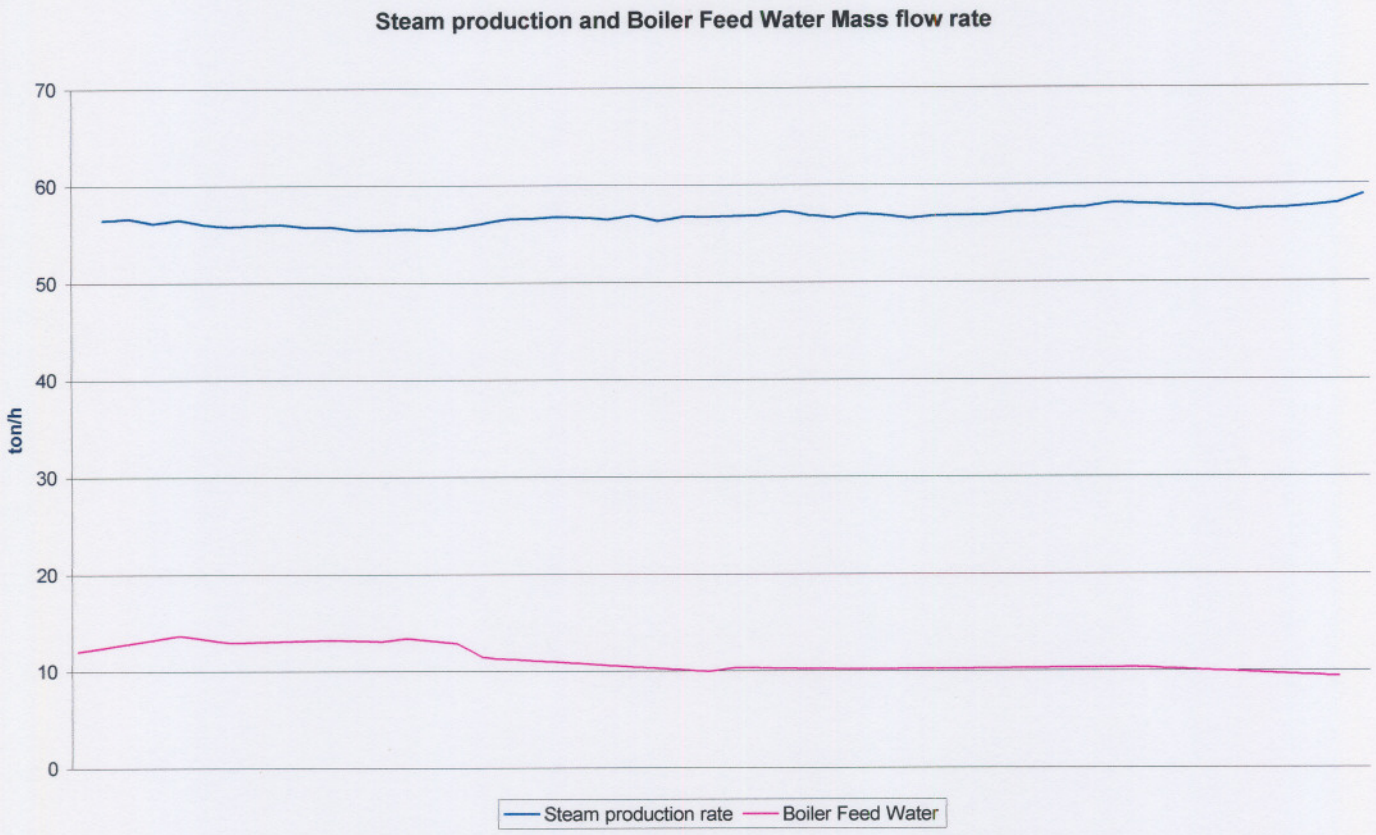

Figure 3.6: Measured Total steam production and boiler feed water mass flow rate for steady-state Gasifier operation.

The average total steam production and boiler feed water mass flow rates is summarised in Table 3-4.

	Ton/h
Steam Production Rate	56.79
Boiler Feed water mass flow rate	11.15

Table 3-4: Average steam production and Boiler feed water mass flow rates

The difference in boiler feed water- and steam production- mass flow rate is big, that points to a possible range of errors during the data acquisition stage. The amount of boiler feed water added to the system should be equal to the amount of steam leaving the system, from a mass balance point of view. Therefore, not much can be learnt about the accuracy of the model when comparing the calculated steam production and boiler feed water rate with the measured values.

3.2 MEASURED RESULTS DISCUSSION

The system total pressure was used to isolate a period of time when the Gasifier was operated at steady state conditions. The average system total pressure differed by 120 kPa from the system operating pressure specified in the simulation model. This was the only period where the system pressure remained relatively constant for a period of 41 minutes. The calculated standard deviation for the system total pressure was 3.2 %, which deems data acquired over this particular period as approximating steady state operating conditions.

The measured volume flow rate in the down-comers was relatively close to one another, with the exception of the measured average volume flow rate through the second down-comer. Flow through the Gasifier cooling system is therefore symmetric. The down comers where accounted for in the simulation model by merging the three down comers into a single down comer, with the geometric properties thereof equal to the sum of the three down-comers combined. From the data presented here, the latter assumption therefore approximates the Gasifier adequately.

The temperature in dam A did not vary considerably, for the period of time considered. The maximum variation in temperature recorded was 1 °C, indicating steady state operation.

The first four water temperature measurements did not differ much from one another that possibly indicates that a mixture of vapour and fluid is present. The variation in the temperature measurement taken at the fifth position can be due to the onset of boiling at this particular position, with the temperature at the sixth-position lower, as expected.

The water temperatures in the down comers follow a similar trend, especially temperatures measured at positions before mixing with the dam A outlet water. This indicates that good mixing takes place in dam A. The difference in temperature measured after mixing took place shows little difference when compared with one another.

The boiler feed water ring main are thus well insulated and temperature losses by convection are thus minimised. The temperatures at the bottom of the down comers are similarly closely related. The largest standard deviation for these measurements is 1.3 %, which indicates steady-state Gasifier operation.

The difference in boiler feed water mass flow rate and total steam production is large and might be to blame on the constant density multiplication factor used with these instruments to give a transient mass flow rate reading. As the temperature varies at the outlet of the Gasifier, the density of the fluid also changes, thus resulting in a possible over/under measurement of the mass of steam produced. As mentioned earlier, the mass of steam leaving the Gasifier should be equal to the amount of boiler feed water added to keep the water level in dam A constant. Therefore, the boiler feed water mass flow rate will only be used to ascertain the accuracy of the simulation model.

The homogeneous two-phase flow simulation model will therefore be verified by means of the following measured parameters:

- Average Volume flow rate measurements in the three down-comers,
- Average Temperature measurement in dam A,
- Average Water temperature measurement at six different locations in the Gasifier jacket annulus at 0.5-meter intervals,
- Average Temperature measurements on the down comer skins at the dam outlet, mixed stream and bottom re-entry inlet temperatures, and
- Average Boiler feed water mass flow rate.

At this point, filtered data is available for the verification of the simulation model under approximated steady state operating conditions. Before comparing the measured and computed results, the results for the Base case configuration 1 simulation will be presented and discussed.

3.3 BASE CASE CONFIGURATION 1 SIMULATION RESULTS

Figure 3.7 summarises the different flow rates, temperatures and total heat transfer rate for the Base case, with the flow in the down comers conforming to configuration 1. The mass flow rates are in kg/s, the temperatures in °C and the heat transfer rate in kW.

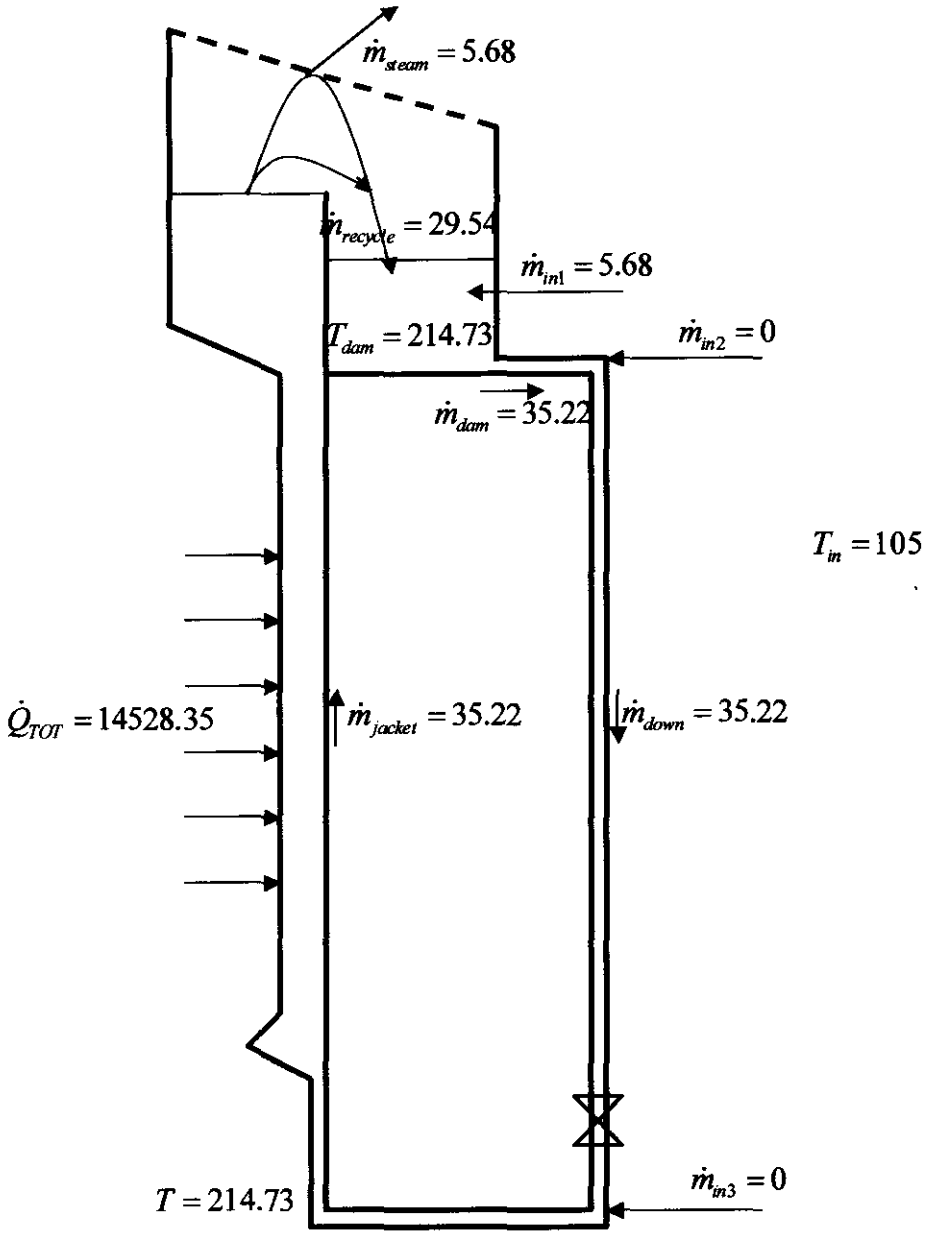

Figure 3.7: Calculated results for the Base Case configuration 1.

It is clear from the figure that mass balance is insured at all points along the flow path including both dams at the top of the jacket. The total heat transfer rate obtained in the jacket is 14.528 MW resulting in a rate of steam production of 5.68 kg/s or 20.45 tons/hr. It is also important to note that for all the results obtained in this study the two-phase heat transfer was in the transition-boiling regime, which is not ideal.

Figure 3.8 to Figure 3.9 show the distribution of quality, temperature, total pressure and density respectively as a function of elevation. From the quality graph it is clear that evaporation starts in the jacket above elevations of -4 m. This can also be seen in the temperature distribution.

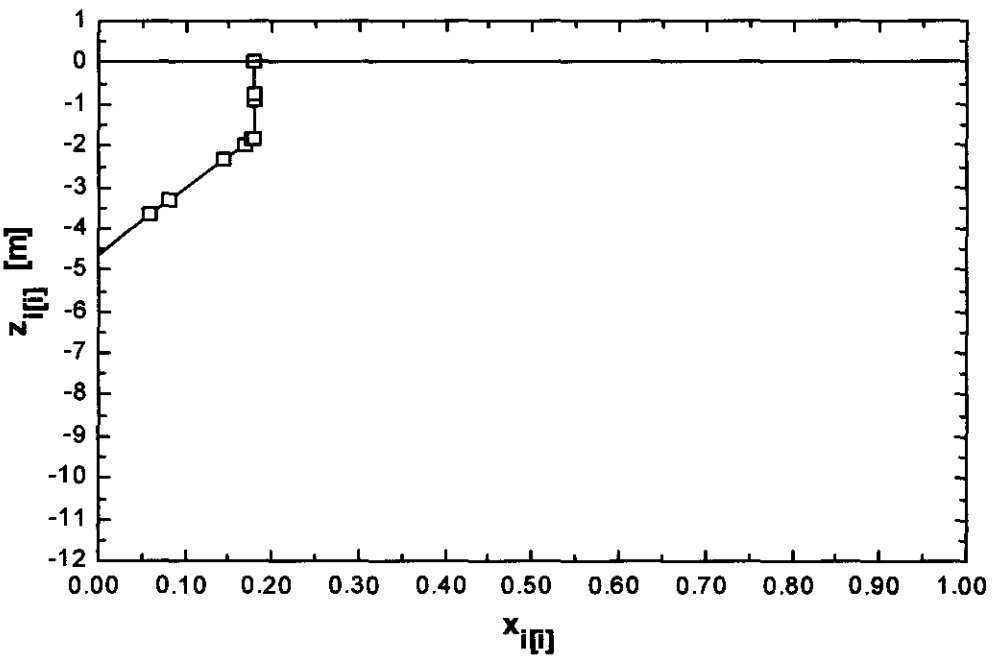

Figure 3.8: Quality versus elevation obtained for the Base Case configuration 1.

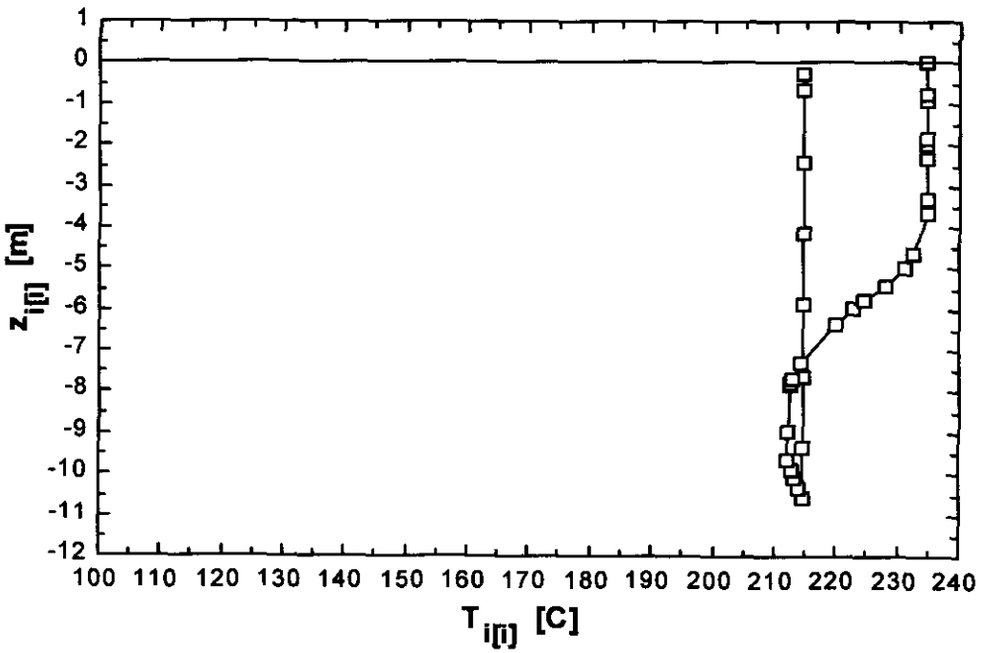

Figure 3.9: Temperature versus elevation obtained for the Base Case configuration 1.

The pressure variation shown in Figure 3.10 includes both the effects of pressure losses and of the increase in pressure due to the depth beneath the surface of the liquid.

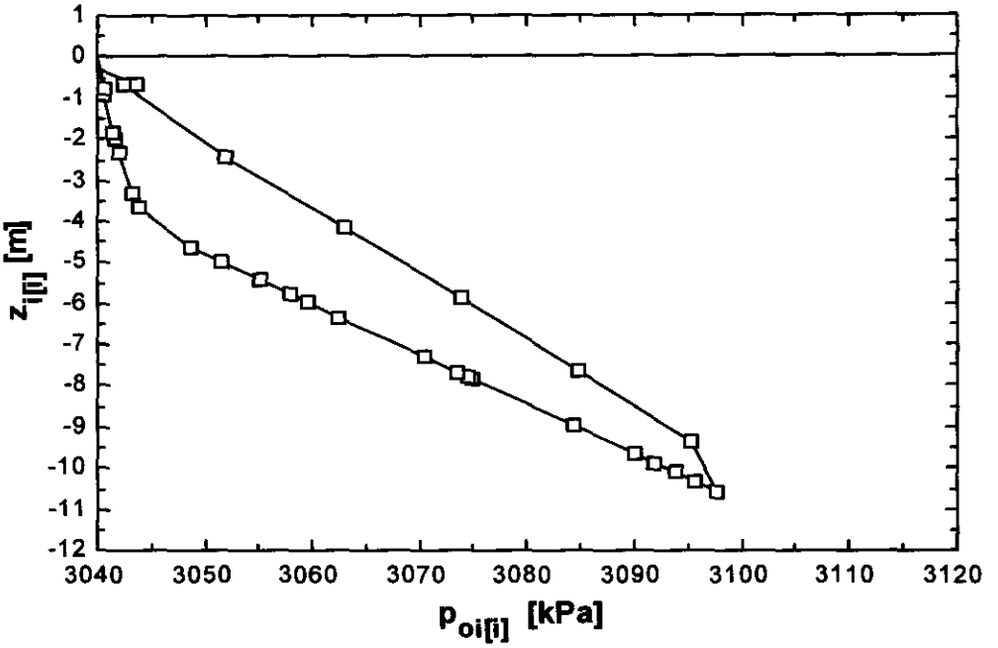

Figure 3.10: Total pressure versus elevation obtained for the Base Case configuration 1.

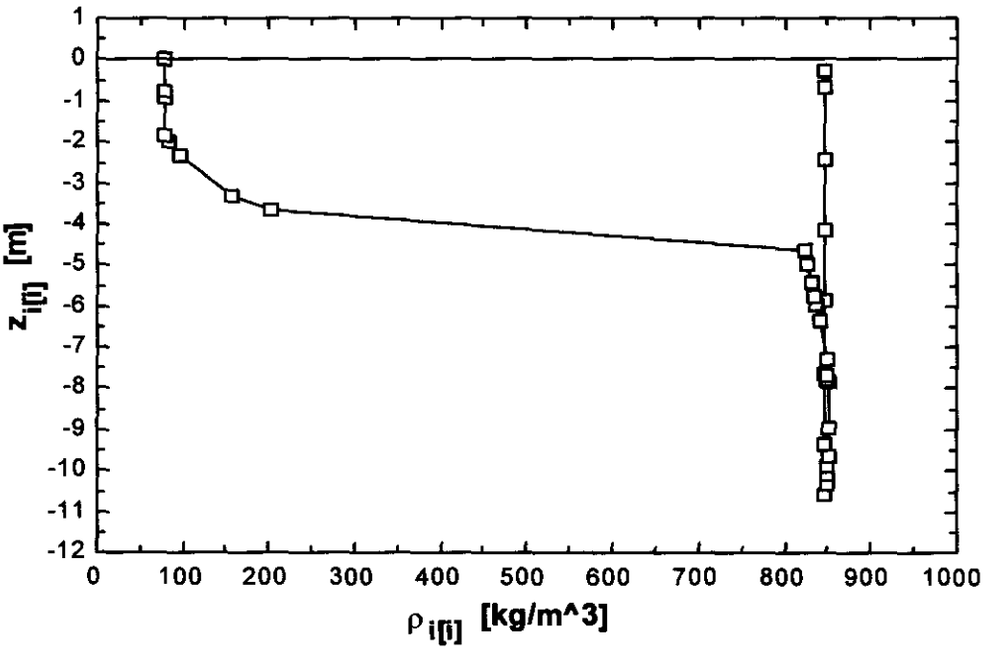

Figure 3.11: Density versus elevation obtained for the Base Case configuration 1.

The variation in density shown in Figure 3.11 also reflects the fact that evaporation starts in the jacket at an elevation above –4 m. This can be seen in the drastic decrease in density as the fraction of steam is increased due to evaporation.

The temperatures in the down-comers are equal to the temperature in dam A, namely 214.73 °C, since it was assumed that the down-comers are well insulated. A small amount of cooling takes place in the jacket at the bottom of the Gasifier where it is colder than at the top of the Gasifier. The liquid in the jacket is then heated gradually due to the increasing Gasifier wall temperature. At an elevation of just above –4 m, the fluid temperature reaches the saturation temperature associated with the local static pressure and evaporation takes place. From this point upwards, the fluid temperature remains approximately constant since in the two-phase region it must be equal to the saturation temperature. The saturation temperature varies only slightly due to the variation in the static pressure, which is determined by the pressure losses and fluid velocities.

The calculated and measured data will next be compared, in order to estimate the accuracy of the simulation model.

3.4 MEASURED AND CALCULATED RESULT COMPARISON

For the purposes of estimating the accuracy of the homogeneous approach, the measured data are compared with calculated data. The overall simulation model accuracy are determined by comparing the following parameters with one another:

- Average Volume flow rate measurements in the three down-comers versus calculated down comer volume flow rate,
- Average Temperature measurement in dam A versus the calculated dam A temperature,
- Average Water temperature measurement at six different locations in the Gasifier jacket annulus at 0.5-meter intervals versus calculated water temperatures coinciding with these positions,
- Average Temperature measurements on the down comer skins at the dam outlet, mixed stream and bottom re-entry inlet temperatures versus calculated water temperatures , and
- Average Boiler feed water mass flow rate versus the calculated boiler feed water mass flow rate.

3.4.1 Down comer volume flow rate comparison

Table 3-5 summarises the comparison between the measured and calculated volume flow rates in the down comers.

	Measured volume flow rate [m^3/h]	Calculated volume flow rate [m^3/h]	Difference [%]
Down Comer 1	25.50	49.88	48.8
Down Comer 2	23.71	49.88	52.4
Down Comer 3	25.86	49.88	49.8
Average volume flow rate per down comer	25.02	49.88	49.8
Total Volume flow rate	75.06	149.634	49.8

Table 3-5: Measured versus Calculated down comer volume flow rate.

Calculated simulation results over estimate the volume flow rate in the down comers by 49.8 %.

3.4.2 Dam A temperature comparison

The comparison between the average measured temperature and the calculated temperature in dam A is shown in Table 3-6.

	Measured Average Temperature [°C]	Calculated Temperature [°C]	Difference [%]
Dam A Temperature	234.83	214.86	8.5

Table 3-6: Measured versus calculated dam A temperature.

It is evident from Table 3-6 that the simulation model under estimates the temperature in dam A by 8.5 %.

3.4.3 *Water Jacket Temperature comparison*

Table 3-7 depicts the comparison between the measured and calculated water temperature in the Gasifier water jacket.

Position	Measured Average Water Temperature [°C]	Calculated Water Temperature [°C]	Difference [%]
Water temp 1	234.19	234.65	0.19
Water temp 2	234.28	234.67	0.16
Water temp 3	234.29	233.61	0.29
Water temp 4	234.31	231.10	1.37
Water temp 5	223.67	222.77	0.43
Water temp 6	218.54	212.54	2.74

Table 3-7: Measured versus calculated water jacket temperature.

The measured and calculated water temperatures in the Gasifier water jacket compares well, as can be seen from Table 3-7.

3.4.4 *Down comer temperature comparison*

Temperatures in the down comers were measured on the pipe surfaces, at three different locations. The first skin thermocouple was placed to measure the water temperature, exiting dam A (D/C Feed Skin). The second skin thermo-couple measured the mixed water temperatures that consist of boiler feed water and water from dam A (D/C Top Temp). The third skin temperature measurement was taken at the point where water enters the bottom of the Gasifier from the down comer (D/C bottom temp). The comparison between the measured and calculated values are shown in Table 3-8.

Position	Measured Temperature [°C]	Average Measured Temperature [°C]	Calculated Water Temperature [°C]	Difference [%]
D/C feed skin 1	232.96	233.50	214.86	7.98
D/C feed skin 2	234.01			
D/C feed skin 3	233.52			
D/C top temp 1	216.15	215.17	214.86	0.14
D/C top temp 2	214.50			
D/C top temp 3	214.86			
D/C bottom temp 1	207.83	207.12	214.87	3.6
D/C bottom temp 2	207.83			
D/C bottom temp 3	205.71			

Table 3-8: Measured and calculated down comer temperature comparison at three different positions.

It is obvious from Table 3-8, that the calculated temperature in the down comers at the various positions remains nearly unchanged. This is due to the assumption that the down comer wall is well insulated, and the temperature only varies due to the increase in total pressure with increasing depth towards the Gasifier bottom. When comparing the difference between the measured and calculated values on a percentage basis, the error margin can be set at approximately 8 %.

3.4.5 *Boiler Feed water mass flow comparison*

Table 3-9 compares the measured boiler feed water mass flow rate with the calculated value.

	Measured mass flow rate [Ton/h]	Calculated mass flow rate [Ton/h]	Difference [%]
Boiler Feed water mass flow rate	11.15	20.40	45.34

Table 3-9: Measured versus Calculated Boiler feed water mass flow rate comparison.

The simulation model over estimates the boiler feed water mass flow rate by 45.3 %, as shown in Table 3-9. As was the case with the measured steam production flow rate, the accuracy of the boiler feed water mass flow rate is also questionable. It is well known that density is a function of temperature, and whether the correct multiplication factor was used to convert the measured mass flow rate is unknown.

3.5 SUMMARY AND DISCUSSION

The total system pressure was used to determine a period of time at which the Gasifier reached steady state conditions. Data conforming to the mentioned criteria was selected that spanned over a period of 41 minutes, and was reduced to average values to enable comparison with the calculated values.

The assumption of symmetrical flow through the Gasifier system is not far off, as can be seen from the measured volume flow rates in the down comers. A large difference in the steam production- and boiler feed water-mass flow rate was observed that points to a possible erroneous density correction factor. The boiler feed water mass flow rate is consequentially used to indicate the accuracy of the simulation model.

The simulation model over estimates the volume flow rate through the down comers by approximately 50 %. It is difficult to accurately specify secondary pressure loss coefficients, and this is suspected to cause the gross over estimation.

Comparison of temperatures in dam A, the water temperature in the cooling water jacket, and water temperatures in the down comers showed a maximum difference of 8 %. This is satisfactory for the purposes of playing the various design concepts off against each other.

The model over estimates the boiler feed water mass flow rate by approximately 45 %, and the reasons could be two-fold. Firstly, a shadow of doubt is cast over the accuracy of the compensation factor used to adjust volume flow rate to mass flow rate during the data acquisition phase. Secondly, the accuracy of the secondary pressure loss coefficients to account for expansions and contractions in the geometry could be to blame.

As mentioned in chapter 1, Uniform homogenous two-phase flow models presume equal gas and liquid velocity. These models offer a simple but important tool for estimation and scaling two-phase flow effects in complex two-phase flow systems. The objective of this study is to determine the effect of the proposed Gasifier cooling water jacket concepts on Gasifier performance. Therefore, a comparison is drawn relative to the un-modified Gasifier or Base case without an emphasis on high model accuracy.

The homogenous or uniform approach has its advantages in ease of implementation. The number of boundary equations and required empirical correlations grow in a near exponential fashion when proceeding from homogenous models towards the more complex two-fluid models with interfacial exchange. However, accuracy is the price paid for the simpler approach, as is evident from the verification process.

With the error margins quantified, and the objective of the study in mind the relative performance evaluation of the Gasifier cooling water jacket concepts relative to the Base case will be presented in the following chapter.

CHAPTER 4: GASIFIER PERFORMANCE EVALUATION RESULTS

4. Introduction

The verification of the simulation model proved that the price paid with a homogeneous two-phase flow approach is accuracy. Temperature calculation along the Gasifier flow path correlated well with the measured data, although the calculation of mass flow rates was inaccurate. Though not much is known about the accuracy of the mass flow measurements as outlined in the previous chapter.

At this point, the purpose of the study still remains to evaluate the different Gasifier cooling water jacket concepts relative to the Base case. The Box Belt-, Belt Jacket A and Belt Jacket B water jackets are compared with the performance of the Base case. Along with each of the mentioned Gasifier water jacket concepts, four different down comer configurations are also analyzed. The effect of the diameter of the holes in the webs of the Belt Jacket A and B concepts are studied parametrically, in order to ascertain the impact thereof on overall Gasifier performance.

The total amount of data generated by the simulation model is enormous that dignifies reflection of the most important performance indicators only. Results for each of the Gasifier cooling water concepts are given schematically. The results are summarized in tabular form, which includes the analyses of the four different down-comer configurations. Performance judgment is made by comparing results relatively to the Base Case, followed by the parametric study results of the effect of hole size on Gasifier performance.

4.1 BASE CASE RESULTS

As mentioned previously, the Base case entails simulation of the un-modified Gasifier as originally used by SASOL. For the sake of completeness, the results of the Base case simulation are shown in Figure 4.1.

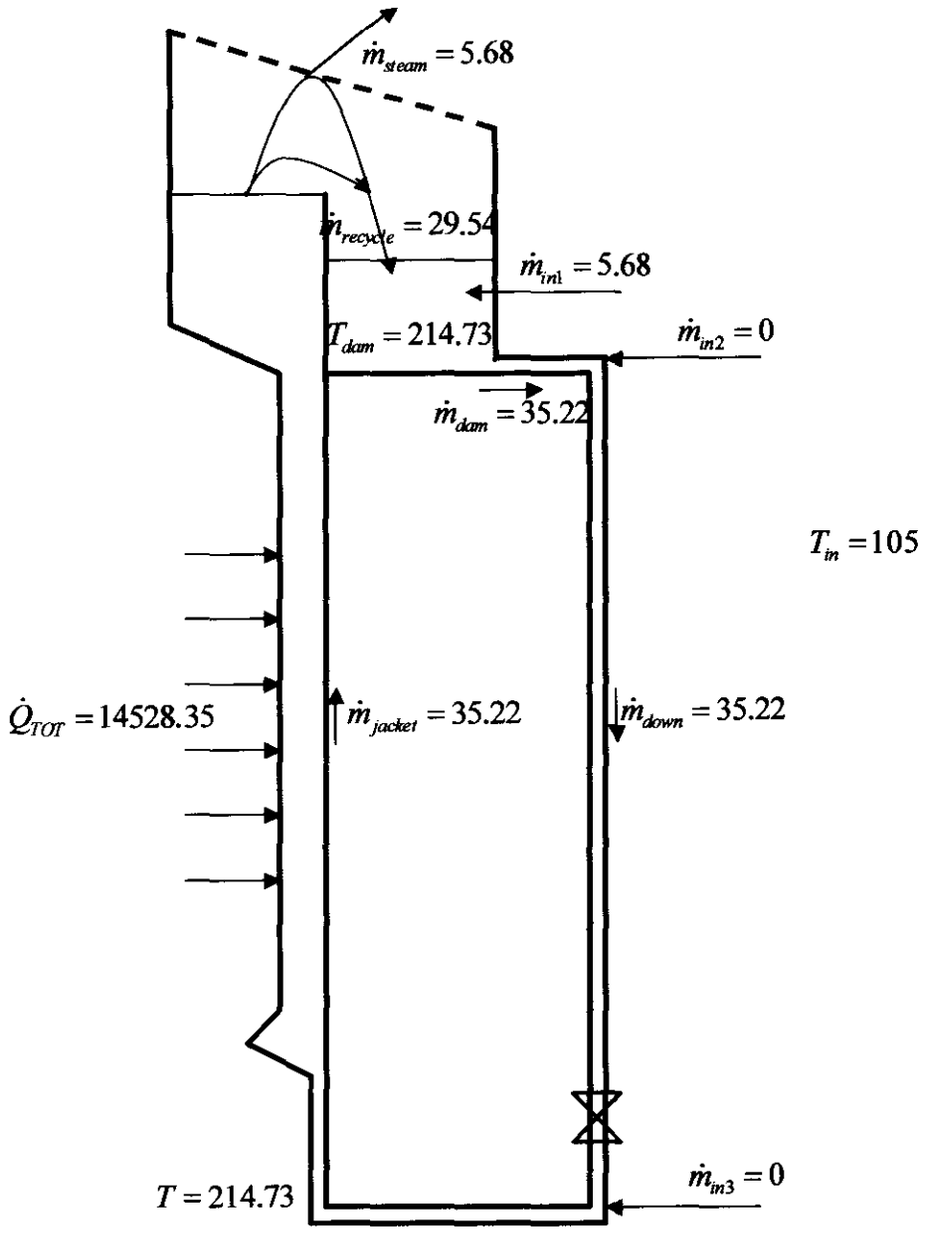

Figure 4.1: Schematic representation of the Base case results.

The mass flow rates are in kg/s, the temperatures in °C and the heat transfer rate in kW. The performance of the Gasifier cooling water jacket concepts is done relatively to the Base case.

4.2 BOX BELT RESULTS

The Box Belt Gasifier jacket consists of a thinner 12 mm thick inner wall, as shown in Figure 1.3.Twenty four vertical channels are welded along the periphery of the Gasifier inner wall, and are interconnected by means of 5 horizontal belts within the cooling water annulus. Calculated results are schematically summarised in Figure 4.2.

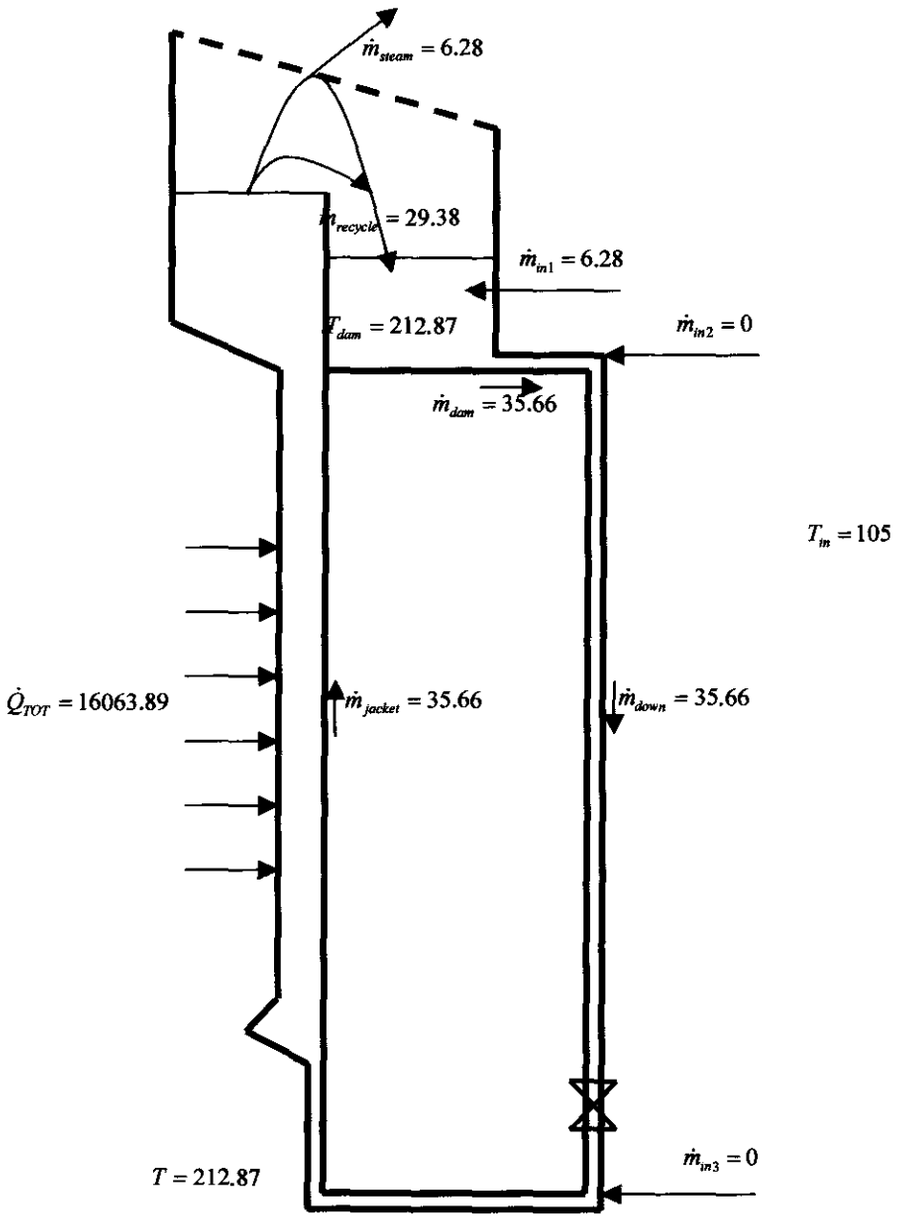

Figure 4.2: Schematic representation of the Box belt results.

4.3 BELT JACKET A RESULTS

The wall thickness with this concept remains 12 mm as with the Box Belt Gasifier Jacket Concept. Five T-shaped stiffener rings are welded horizontally along the periphery of the Gasifier inner wall and the web of the T-sectioned stiffening rings in the cooling water annulus. A number of holes are drilled through the web of the T-section in an effort to minimise pressure loss across the stiffening rings. The results for the Belt Jacket A cooling water jacket concepts is summarized in Figure 4.3.

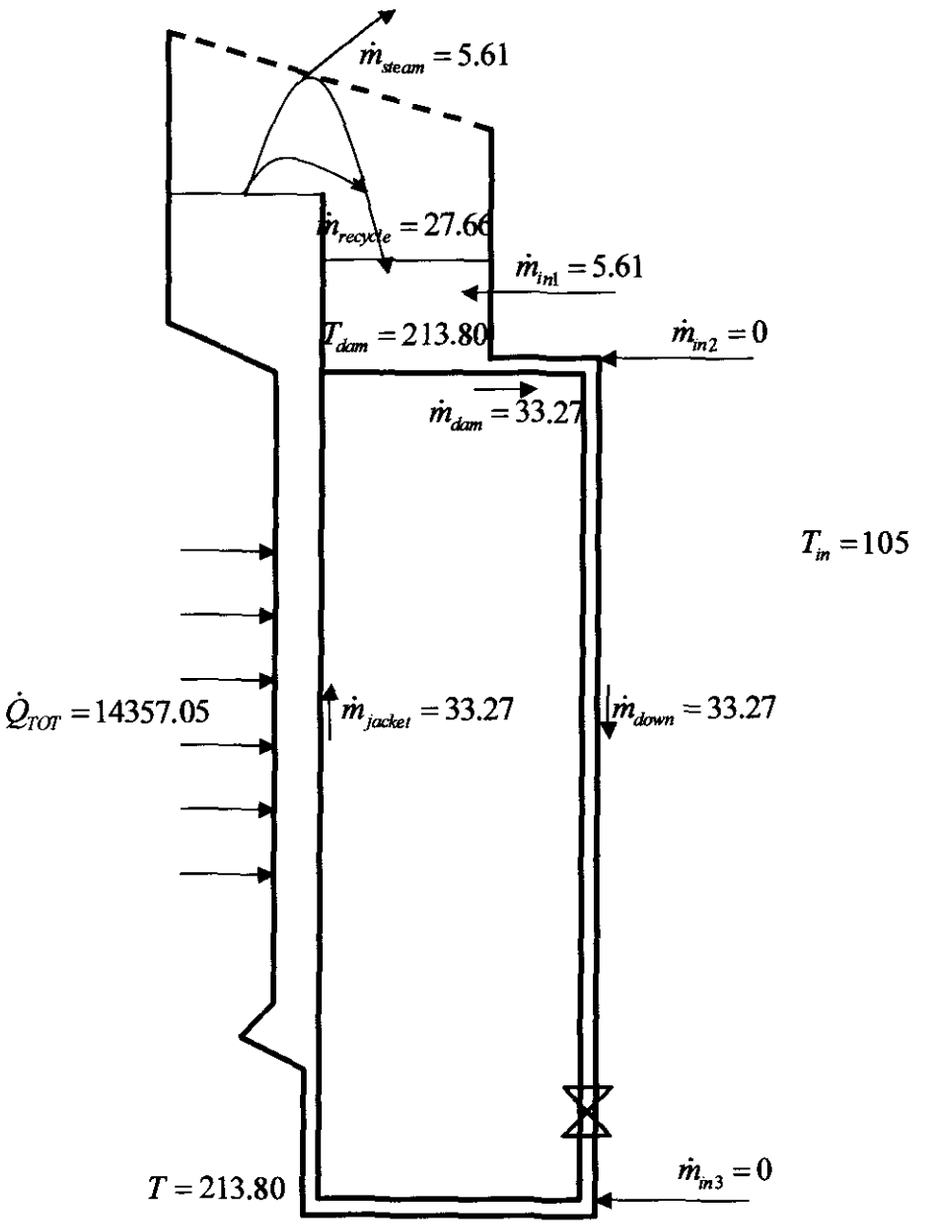

Figure 4.3: Schematic representation of the Belt Jacket A results

4.4 BELT JACKET B RESULTS

As with the previous concepts, the inner wall thickness of the Gasifier jacket remains 12 mm thick. Five Channel shaped stiffener rings are welded horizontally along the Gasifier inner wall periphery and channel flanges in the cooling water jacket annulus. A number of holes are drilled through both flanges of the stiffening rings to minimise the induced pressure loss by the additional stiffening rings. Results for the Belt Jacket A concept is schematically represented in Figure 4.4.

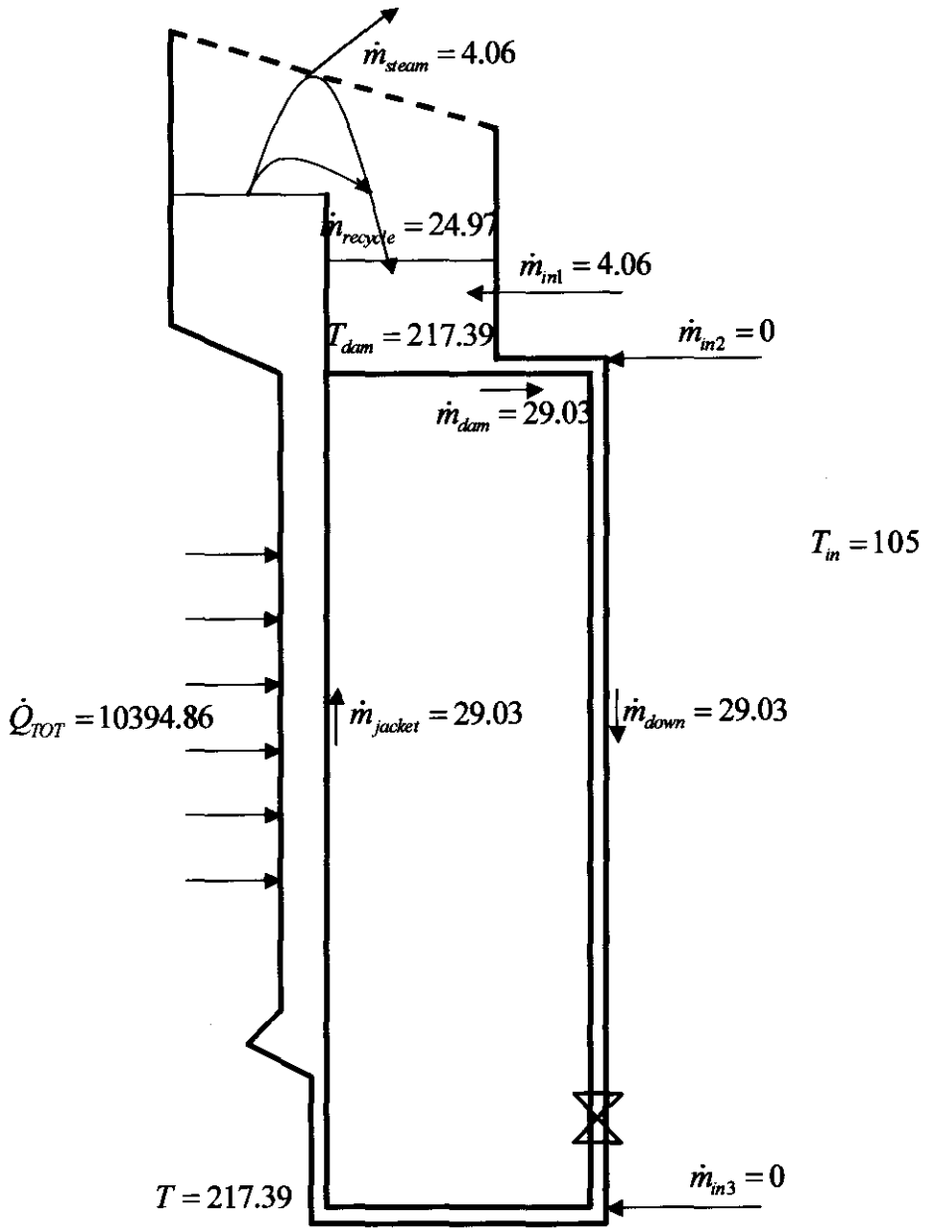

Figure 4.4: Schematic representation of the Belt Jacket B results.

4.5 SUMMARY OF RESULTS FOR ALL THE CONFIGURATIONS

In order to ascertain the difference in the performance of the Gasifier cooling water jacket concepts and down comer configurations, the most important calculated parameters are summarized in Table 4-1. This includes heat transfer- and steam production-rates as well as down comer flow rates and temperature in dam A.

Water Jacket Concept	Down comer configuration	$\dot{Q}_{TOT}$ [MW]	$\dot{m}_{steam}$ [tons/hr]	$\dot{m}_{steam}$ [kg/s]	$\dot{m}_{jacket}$ [kg/s]	$\dot{m}_{down}$ [kg/s]	T_{dam} °C
Base Case	Configuration 1	14.5	20.4	5.7	35.2	35.2	214.7
	Configuration 2	14.5	20.4	5.7	35.2	35.2	234.7
	Configuration 3a	14.7	20.7	5.8	38.7	32.9	234.7
	Configuration 3b	4.3	6.6	1.8	1.8	0.0	234.7
Box Belt	Configuration 1	16.1	22.6	6.3	35.7	35.7	212.9
	Configuration 2	16.1	22.6	6.3	35.6	35.6	234.7
	Configuration 3a	16.4	23.6	6.6	39.8	33.3	234.7
	Configuration 3b	5.1	7.8	2.2	2.2	0.0	234.7
Belt Jacket A	Configuration 1	14.4	20.2	5.6	33.3	33.3	213.8
	Configuration 2	14.4	20.2	5.6	33.2	33.2	234.7
	Configuration 3a	14.5	20.4	5.7	36.3	30.6	234.7
	Configuration 3b	4.6	7.1	2.0	2.0	0.0	234.7
Belt Jacket B	Configuration 1	10.4	14.6	4.1	29.0	29.0	217.4
	Configuration 2	10.4	14.6	4.1	29.0	29.0	234.7
	Configuration 3a	14.4	20.3	5.6	34.8	29.1	234.7
	Configuration 3b	4.6	7.1	2.0	2.0	0.0	234.7

Table 4-1: Summary of the most important parameters calculated for all the Gasifier water jacket concepts and down comer configurations.

Closer inspection of Table 4-1, reveals increased performance of the Box Belt water jacket concept. The overall heat transfer rate and steam production is better in comparison with the Base case and other concepts. In order to simplify the interpretation, results are viewed qualitatively by comparing the different configurations.

For this reason, Table 4-2 represents the relative values of heat transfer rate, steam production rate and jacket flow rate when compared to the Base Case.

		$\dot{Q}_{TOT}$	$\dot{m}_{steam}$	$\dot{m}_{jacket}$
Base Case	Configuration 1	1.00	1.00	1.00
	Configuration 2	1.00	1.00	1.00
	Configuration 3a	1.01	1.01	1.10
	Configuration 3b	0.30	0.32	0.05
Box Belt	Configuration 1	1.11	1.11	1.01
	Configuration 2	1.11	1.11	1.01
	Configuration 3a	1.13	1.15	1.13
	Configuration 3b	0.35	0.38	0.06
Belt Jacket A	Configuration 1	0.99	0.99	0.94
	Configuration 2	0.99	0.99	0.94
	Configuration 3a	1.00	1.00	1.03
	Configuration 3b	0.32	0.35	0.06
Belt Jacket B	Configuration 1	0.72	0.71	0.82
	Configuration 2	0.72	0.71	0.82
	Configuration 3a	0.99	0.99	0.99
	Configuration 3b	0.32	0.35	0.06

Table 4-2: Results obtained for the heat transfer rate, steam production rate and jacket flow rate relative to the Base case configuration 1.

From Table 4-2 it can be seen that for the Base Case there is very little difference between configurations 1 and 2. The only real difference is in the dam temperature, since the boiler feed water is either added in the dam or just below the dam in the down-comer. Any difference in flow rates will only be due to the slight difference in pressure losses in the inlet to the down-comer due to differences in water temperature and therefore density.

For all the concepts the maximum jacket flow rate and heat transfer is obtained with configuration 3a. The reason for the good performance of this configuration is that although much the same temperature conditions are obtained in the cooling jacket, the flow rate in the down-comers is much smaller resulting in smaller pressure losses and therefore substantially higher overall flow rates. The higher flow rates in turn, result in higher heat transfer coefficients and therefore better heat transfer and steam production rates.

For all the concepts, the worst case is for configuration 3b where the entire volume of boiler feed water added at the bottom of the jacket is evaporated. The reason for this is that the jacket flow rates are very low because densities are low with so much steam present, with associated low heat transfer rates.

The jacket mass flow rate for the Box Belt configuration is very close to that of the Base Case. In fact it is one per cent higher even though at first glance it contains many more flow restrictions and area variations. However, the Gasifier wall is much thinner in this case, resulting in a wider effective cross-sectional flow area. Although the flow rate is only one per cent higher, the resultant heat transfer rate is 11 percent more. This is mainly due to the extended heat transfer areas provided by the added stiffener elements in the Box Belt concept.

The flow rates in both the Belt Jacket configurations are less than in the Base Case and more so in Belt Jacket B than in Belt Jacket A. This is due to the presence of the holes in the stiffener rings which act as orifices in the flow path. Belt Jacket B is affected more since it has twice the number of orifices in series than Belt Jacket A. However, due to the extended heat transfer areas, the heat transfer rate in Belt Jacket A ends up very close to that of the Base Case despite the lower flow rates. In Belt Jacket B however, the much lower flow rate adversely affects the heat transfer rate despite the extended heat transfer areas.

4.6 EFFECT OF HOLE SIZE ON GASIFIER PERFORMANCE

These last two results show the need for a parametric study to determine the influence of the hole sizes on the performance of the cooling jacket for Belt Jackets A and B. Such parametric studies were therefore conducted for both Belt Jackets A and B using configuration 3a which initially gave the most promising performance results.

Figure 4.5 shows the jacket mass flow rates obtained for the Belt Jacket A configuration 3a for different hole sizes between 8 mm and 30 mm while Figure 4.6 shows the resultant heat transfer rates. From the figures it is clear that an improvement of less than a half per cent is obtained when the hole size is increased from 20 mm to 30 mm. However, a sharp reduction in performance is observed at hole sizes below 20 mm. The original choice of 20 mm therefore seems to be very close to the optimum value.

The shape of the holes will have only a very small influence on the C_d value assumed in the simulation model if it does not deviate too much from a circular shape and the total effect can therefore be assumed to be negligible.

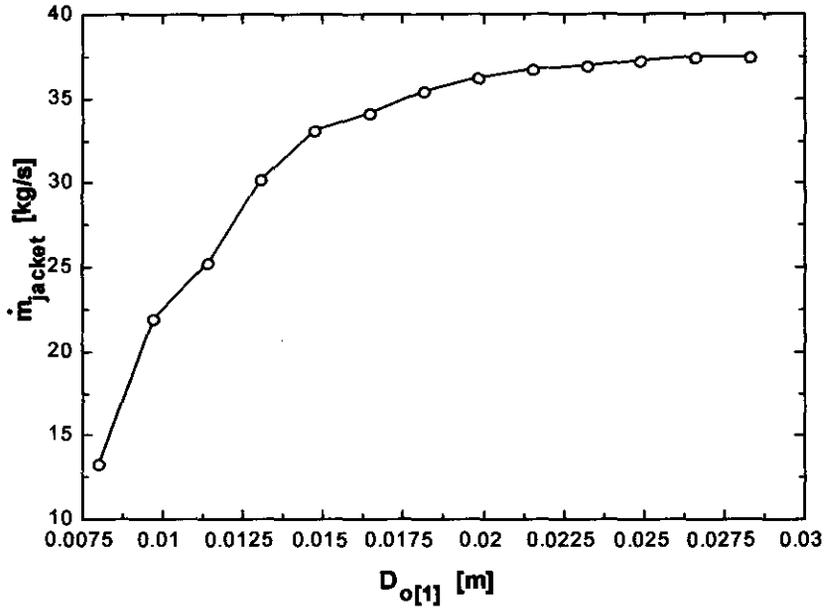

Figure 4.5: Effect of the hole size on the jacket mass flow rate for Belt Jacket A configuration 3a.

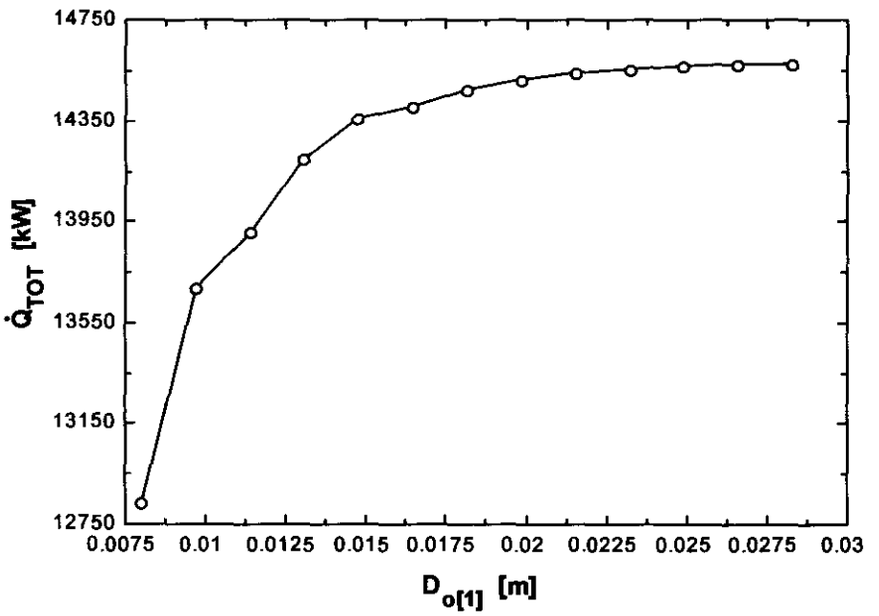

Figure 4.6: Effect of the hole sizes on the heat transfer rate for Belt Jacket A configuration 3a.

Figure 4.7 and Figure 4.8 show the results of jacket mass flow and heat transfer rate versus hole size for the Belt Jacket B concept configuration 3a.

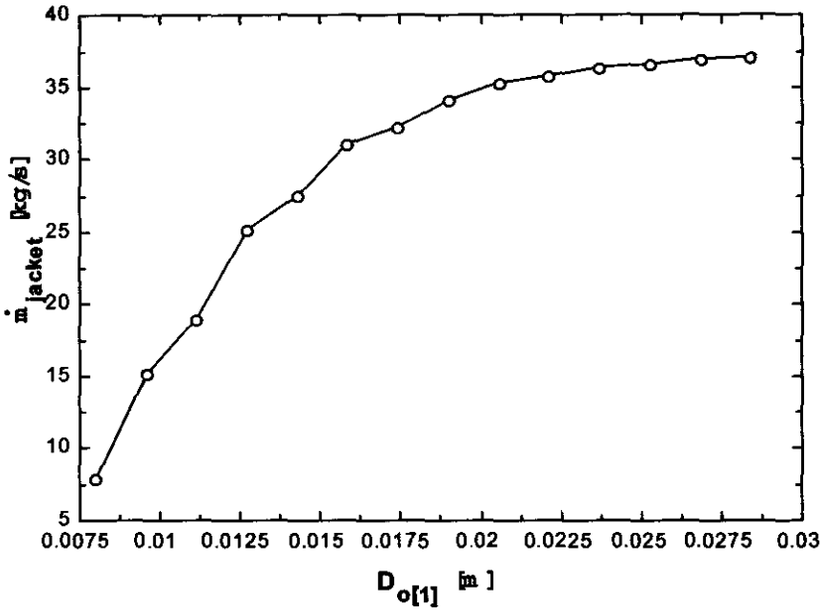

Figure 4.7: Effect of the hole sizes on the jacket mass flow rate for Belt Jacket B configuration 3a.

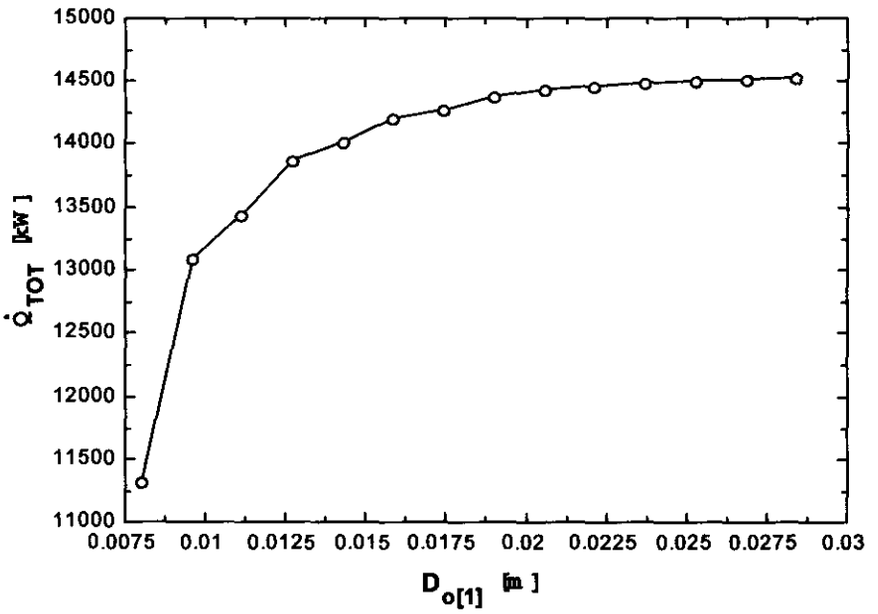

Figure 4.8: Effect of the hole sizes on the heat transfer rate for Belt Jacket B configuration 3a.

The figures show that an improvement of less than one per cent is obtained when the hole size is increased from 20 mm to 30 mm. The original choice of 20 mm therefore also seems to be very close to the optimum value for this case.

4.7 CONCLUSION AND RECOMMENDATIONS

Results for the Base Case gave heat transfer and steam production rates that are 70 percent higher than the specified nominal design value. This difference may be due to a number of factors including the difficulty in specifying accurate pressure loss coefficients; Gasifier wall temperatures and heat transfer correlations for the specific geometry. However, in practice the actual steam production rate obtained via measurements also vary substantially below and above the nominal rate. One should concentrate on the relative values when comparing different design configurations. The variations in heat transfer rate are due to a complex combination of flow rate, efficiency of extended heat transfer areas as well as complex boiling heat transfer correlations. It is also important to note that for all the results obtained in this study the two-phase heat transfer was in the transition-boiling regime, which is not ideal.

From the results it is clear that for all the concepts, configuration 3a seems the most promising while configuration 3b showed the poorest performance. Of all the concepts the Box Belt provides the best performance and Belt Jacket B the poorest performance. Heat transfer- and steam production-rates for the Box Belt configuration 3a is approximately 15 percent higher than for the Base Case configuration 1.

However, from a structural point of view, the Belt Jacket concepts are probably the most ideal. Fortunately, for the Belt Jackets, configuration 3a shows fluid flow and heat transfer performance comparable with that of the Base Case.

The parametric study for the hole sizes in the case of the Belt Jacket configurations showed that performance improvements of less than a one per cent is obtained when the hole size is increased from 20 mm to 30 mm. However, a sharp reduction in performance is observed at hole sizes below 20 mm. The shape of the holes will have only a very small influence if it does not deviate too much from a circular shape and the total effect can therefore be assumed to be negligible.

Based on these results the following are recommended:

- If possible the Box Belt concept combined with configuration 3a should be employed since it will provide the best performance, which is approximately 15 percent higher than the Base Case.
- Configuration 1 and 2 could also be used with the Box Belt and Belt Jacket A concepts since it should provide performance comparable to the Base Case.
- If the Belt Jacket B concept is implemented, only configuration 3a will provide performance comparable to that of the Base Case.
- Configuration 3b should not be implemented at all, since for all the concepts it results in a significant reduction in performance, up to as much as 68 percent.
- The hole size should be maintained at 20 mm for the specified 300 holes per flange since it is close to the optimum value.

CHAPTER 5: CONCLUSION

5. Research Conclusion

Three main simulation approaches can be identified with increasing complexity namely Uniform homogenous two-phase flow models, Separated two-phase flow models with no interface exchange, Drift flux and Separated two-phase flow models with interface exchange. The uniform homogenous simulation approach was chosen due to the relative ease of implementation offered.

Homogenous two-phase flow does not have to deal with gas-liquid interfacial interactions. The fact that homogenous conservation equations are derived from equations similar to single-phase flow implies that empirical correlations for single-phase flow can be employed. Therefore, no new boundary conditions have to be defined for a homogenous/uniform property computer code.

The principal shortcoming is presuming equal gas- and liquid- velocities as well as equal gas- and liquid-temperatures. However, if implemented correctly, this model can be valuable in estimation/scaling of complex system behaviour. Verification of the simulation model proved inaccuracy prevailed in the calculation of steam production- and boiler feed water-mass flow rates. This may be due to difficulty in accurately specifying accurate pressure loss coefficients; Gasifier wall temperatures and heat transfer correlations for the specific geometry.

The total system pressure was used to determine a period of time at which the Gasifier reached steady state conditions. Data conforming to the mentioned criteria was selected that spanned over a period of 41 minutes, and was reduced to average values to enable comparison with the calculated values.

The assumption of symmetrical flow through the Gasifier system is not far off, as can be seen from the measured volume flow rates in the down comers. A large difference in the steam production- and boiler feed water-mass flow rate was observed that points to a possible erroneous density correction factor. The boiler feed water mass flow rate is consequentially used to indicate the accuracy of the simulation model.

The simulation model over estimates the volume flow rate through the down comers by approximately 50 %. It is difficult to accurately specify secondary pressure loss coefficients, and this is suspected to cause the gross over estimation.

Comparison of temperatures in dam A, the water temperature in the cooling water jacket, and water temperatures in the down comers showed a maximum difference of 8 %. This is satisfactory for the purposes of playing the various design concepts off against each other.

The model over estimates the boiler feed water mass flow rate by approximately 45 %, and the reasons could be two-fold. Firstly, a shadow of doubt is cast over the accuracy of the compensation factor used to adjust volume flow rate to mass flow rate during the data acquisition phase. Secondly, the accuracy of the secondary pressure loss coefficients to account for expansions and contractions in the geometry could be to blame.

As mentioned, Uniform homogenous two-phase flow models presume equal gas and liquid velocity. These models offer a simple but important tool for estimation and scaling two-phase flow effects in complex two-phase flow systems. The objective of this study is to determine the effect of the proposed Gasifier cooling water jacket concepts on Gasifier performance. Therefore, a comparison is drawn relative to the un-modified Gasifier or Base case without an emphasis on high model accuracy.

The homogenous or uniform approach has its advantages in ease of implementation. The number of boundary equations and required empirical correlations grow in a near exponential fashion when proceeding from homogenous models towards the more complex two-fluid models with interfacial exchange. However, accuracy is the price paid for the simpler approach, as is evident from the verification process.

Researchers still rely heavily on empirical relations, making the simulation of a two-phase flow system application specific. These empirical relations are furthermore obtained under steady state conditions, which further contribute to inaccuracy.

predicting system behaviour on a macroscopic scale.